Investigation of phonon excitations in ^{114}Cd with the $(n, n'\gamma)$ reaction

D. Bandyopadhyay,[1,*] S. R. Lesher,[1,†] C. Fransen,[1,‡] N. Boukharouba,[1,§] P. E. Garrett,[2] K. L. Green,[2] M. T. McEllistrem,[1] and S. W. Yates[1,3]

[1]*Department of Physics and Astronomy, University of Kentucky, Lexington, Kentucky 40506-0055*

[2]*Department of Physics, University of Guelph, Guelph, Ontario N1G2W1, Canada*

[3]*Department of Chemistry, University of Kentucky, Lexington, Kentucky 40506-0055*

(Received 29 August 2007; published 8 November 2007)

Properties of low-spin states in ^{114}Cd have been studied with the $(n, n'\gamma)$ reaction. Gamma-ray angular distributions and excitation functions have been used to characterize the decays of the excited levels. Level lifetimes have been obtained with the Doppler-shift attenuation method. Sixteen new levels and many new transitions have been suggested below 3.5 MeV in excitation energy. Levels belonging to the phonon multiplets have been proposed based on their decay patterns and collectivity, and the existing intruder structure has been extended. A two-phonon 1^+_{ms} state has been suggested. Excitation of the hexadecapole moment has been considered. Data have been compared with the theoretical calculations of the interacting boson model.

DOI: 10.1103/PhysRevC.76.054308 PACS number(s): 27.60.+j, 21.10.Hw, 21.10.Tg, 23.20.Lv

I. INTRODUCTION

The stable even-even Cd nuclei are known to exhibit a complex structure that cannot be understood in the framework of the simple anharmonic vibrator. Even the concept of the coexistence of a deformed intruder configuration and comparably less-deformed "normal" phonon states with strong mixing fails to explain all the experimental observables (e.g., the energy levels as well as the $B(E2)$ values [1–7]). A better description of the low-spin states at lower excitation energy has been achieved by considering the neutron-proton version of the interacting boson model (IBM-II) [8–10], but the enigmatic behavior of these states in the Cd nuclei still calls for more experimental and theoretical attention.

In the Cd nuclei, the presence of additional 0^+ and 2^+ states near the two-phonon triplet makes the phonon structure ambiguous. It has been found that, in some cases, even assigning a clear two-phonon triplet is a challenge. Systematic studies over the chain of Cd isotopes reveal [11] that the 0^+ states show the expected V-shaped behavior with excitation energy and suggest an intruder origin for the 0^+ states. However, the strong $E2$ transitions from these states to the first excited states (2^+_1) indicate their phonon character. The low-lying states in ^{114}Cd have been studied previously with a variety of different probes, and the spins and parities of these states are generally well characterized [1,12–14]. Regan *et al*. [15] suggested that the structure of the Cd nuclei changes from vibrator to rotor around spin 10–12$\hbar$. According to them, the Cd isotopes show vibrational characteristics at low spin and, once the system obtains deformed shape, rotational motion may become favored.

Three-phonon structures have been observed in ^{108}Cd [16], ^{110}Cd [17,18], ^{112}Cd [19], ^{116}Cd, and ^{118}Cd [20] isotopes and have been suggested for ^{114}Cd [1,13]. There are indications that, in case of ^{114}Cd, it may be possible to extend the level scheme up to the four-phonon level; however, the lifetimes obtained from the γ-ray induced Doppler (GRID) technique [1] are sometimes complicated by feeding from the higher lying levels and the Coulomb excitation [13] involves complex model dependence, resulting in larger uncertainties for the transition strengths. We have studied ^{114}Cd with monoenergetic neutrons through the $(n, n'\gamma)$ reaction. In this reaction, population of the level of interest through selection of the appropriate neutron energy results in a more accurate measurement of the level lifetime. The complete quadrupole-octupole coupled multiplet and the fragmented first mixed-symmetry states have been reported earlier [21,22]. In this paper, we present the results of our search for higher phonon states.

II. EXPERIMENTAL DETAILS AND RESULTS

Low-lying states of ^{114}Cd have been studied at the University of Kentucky 7-MV accelerator facility through the inelastic scattering of fast neutrons. A pulsed proton beam (with pulse width ~1 ns and frequency ~2 MHz) with a current of about 2 μA was passed into a cylindrical gas cell with a length of 3.0 cm and a diameter of 1.0 cm filled with tritium gas at nearly one atmosphere pressure. A molybdenum foil with a thickness of 8 μm served as a window to the gas cell. Monoenergetic neutrons with an energy spread of about 60 keV were produced through the ^{3}H$(p, n)^3$He reaction. The scattering sample, 13 pieces of metallic ^{114}Cd (isotopic enrichment 98.55%) totaling 47.835 g, was arranged within a cylindrical polyethelene container 1.8 cm in diameter and 3.6 cm in height. This sample was suspended in the neutron flux at a distance of 5 cm from the end of the gas cell.

*Present address: TRIUMF, 4004 Wesbrook Mall, Vancouver, BC V6T2A3, Canada; dipa@triumf.ca

†Present address: Department of Physics, University of Richmond, Richmond, VA 23173, USA.

‡Present address: Institut für Kernphysik, Universität zu Köln, D-50937 Köln, Germany.

§Present address: 75 Rue Benbrouk Hocine, Heliopolis, Guelma 24000, Algeria.

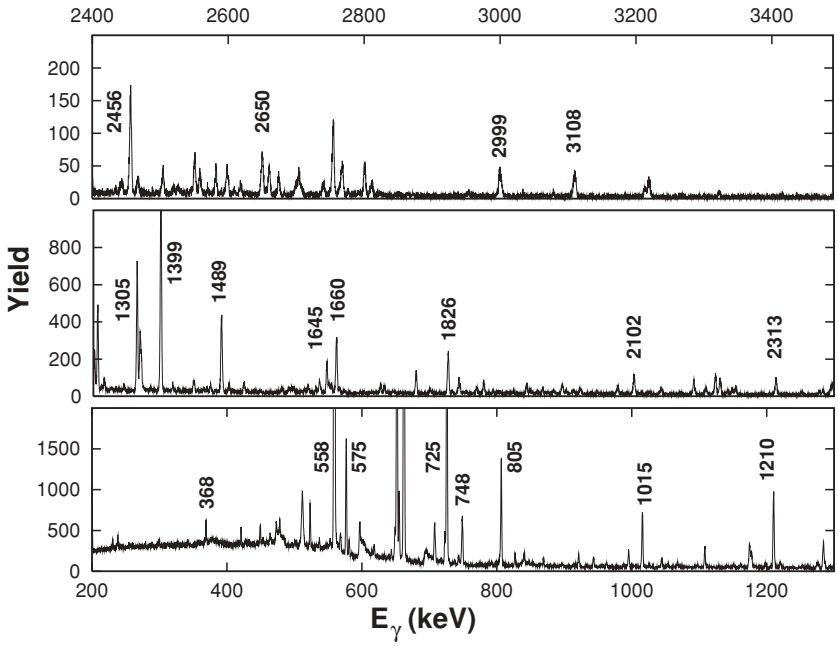

FIG. 1. Gamma-ray spectrum obtained with the ^{114}Cd$(n, n'\gamma)$ reaction at a neutron energy of 3.5 MeV and at a detection angle of 90°. Peaks labeled with energies in keV are from ^{114}Cd.

The γ rays emitted in the ^{114}Cd$(n, n'\gamma)$ reaction were recorded with a Compton-suppressed HPGe detector with a relative efficiency of 55% compared to that of a 7.6 × 7.6 cm NaI detector. An annular BGO shield was used for Compton suppression. The HPGe and BGO detectors were at a distance of 115 cm from the scattering sample and were further shielded by boron-loaded polyethylene, copper, and tungsten. Time-of-flight gating was implemented to suppress the background radiation and, hence, to improve the quality of the spectra. The neutron fluences were monitored by a BF_3 proportional counter fixed at 90° relative to the axis of the incident beam and at a distance of 3.78 m from the gas cell. The neutron flux was further monitored by observing the time-of flight spectra of neutrons in a fast liquid scintillator (NE218) at an angle of 43° relative to the incident beam axis and at a distance of 5.9 m from the gas cell. Energy and efficiency calibrations of the HPGe detector were performed with a ^{226}Ra radioactive source. More detailed descriptions of the experimental setup may be found elsewhere [23,24].

The γ-ray yields from different levels in ^{114}Cd were measured over the range of neutron energies from 1.9 to 3.8 MeV in 0.1 MeV steps. Figure 1 shows a typical spectrum of the γ rays obtained at an angle of 90° with 3.5-MeV neutrons. Intense transitions from ^{114}Cd are labeled accordingly.

Excitation functions of a few selected γ rays are shown in Fig. 2. The excitation function data were used to place the γ rays in the level scheme and for tentative spin assignments. In this figure, the 742-keV γ ray clearly shows two thresholds, one at 2048 keV and another near 2701 keV. The 1251-keV γ ray is new and is reported for the first time; it has a threshold at ∼2.5 MeV. The very slow rise in the excitation function suggests higher spin for the level of origin of this γ ray, and from the energy balance we assign this γ ray to the 2535-keV 5^- level. The fast rise and fall in the excitation functions of the 1315- and 1879-keV γ rays support their 2^+ and 0^+ assignments, whereas the more gradual slope for 1645-keV γ ray supports its 3^+ origin.

To study the angular distributions of γ rays emitted in the ^{114}Cd$(n, n'\gamma)$ reaction, spectra were recorded at 11 different angles from 40° to 150° and at neutron energies of 2.5, 3.0, and 3.5 MeV. In these experiments, the energy calibration

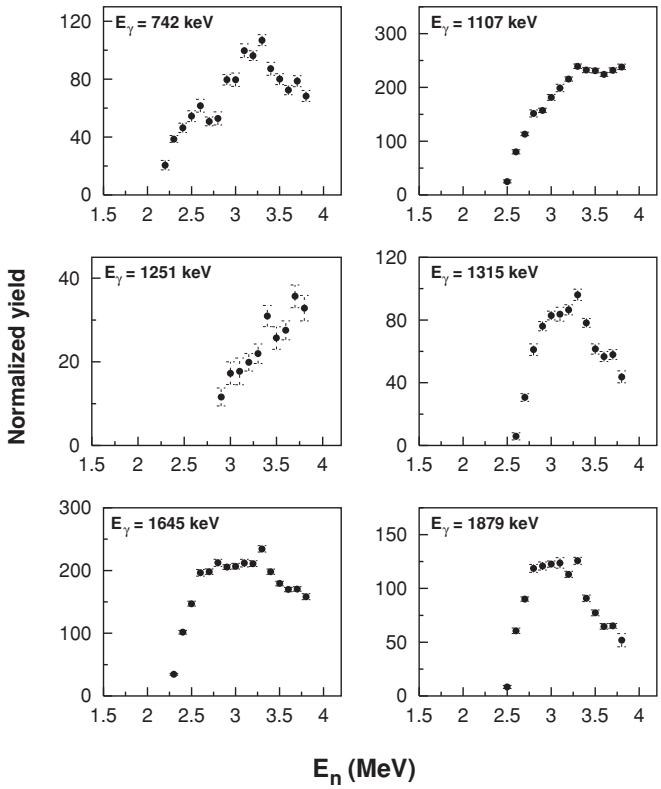

FIG. 2. Gamma-ray yield as a function of neutron energies obtained in the ^{114}Cd$(n, n'\gamma)$ reaction at a detection angle of 90°.

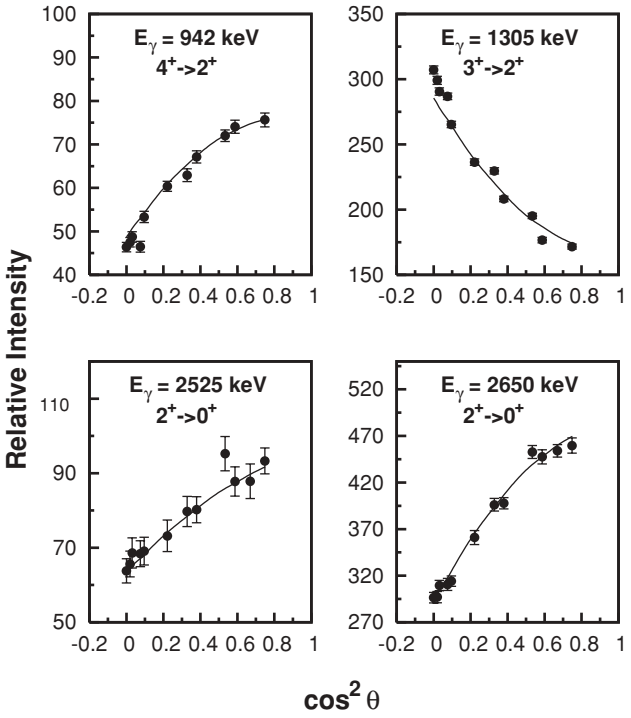

FIG. 3. Angular distributions of selected γ rays observed in the ^{114}Cd$(n, n'\gamma)$ reaction. Solid lines are fits to the data.

of the HPGe detector was continuously monitored with the 661.6-, 1368.6- and 2754.0-keV γ rays from ^{137}Cs and ^{24}Na radioactive sources.

The angular distributions of the γ rays were fit to even-order Legendre polynomial expansions of the form

$$W(\theta) = I_\gamma[1 + a_2 P_2(\cos\theta) + a_4 P_4(\cos\theta)], \qquad (1)$$

where I_γ is the angle-averaged γ-ray intensity, P_l are Legendre polynomials, and a_2 and a_4 are the angular distribution coefficients. The data were then compared to theoretical predictions calculated with the code CINDY [25] to determine the multipolarities of the decay transitions. Figure 3 shows the angular distributions of some selected γ rays. The values of the $E2/M1$ mixing ratios (δ) and the branching ratios of the transitions are given in Table I; Table II displays the calculated transition strengths.

Lifetimes of the low-lying excited states have been extracted from the angular distribution data by considering the Doppler shifts of the γ rays with angle. The position of the centroid of the γ-ray peak, $E_\gamma(\theta)$, at an emission angle θ relative to the incident neutrons can be described as [26]

$$E_\gamma(\theta) = E_\circ\left(1 + F(\tau)\frac{v_{\rm cm}}{c}\cos\theta\right), \qquad (2)$$

where $E_\circ$ is the unshifted γ-ray energy and $F(\tau)$ is the Doppler-shift attenuation factor. The observed energies of the 2799.9-, 2456.0- and 2218.8-keV γ rays as a function of emission angle are shown in Fig. 4. The straight lines are the fits to the experimental data from which the $F(\tau)$ values have been determined. Lifetimes have been obtained by a comparison of the experimental $F(\tau)$ values of Fig. 4 with those calculated following the nuclear stopping theory of Winterbon [27,28].

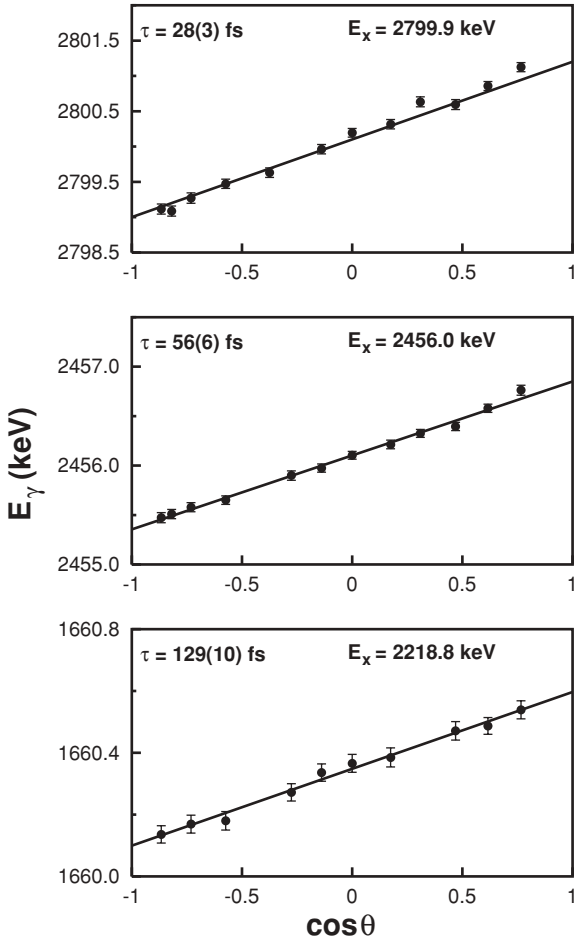

FIG. 4. Shift in γ-ray energies as a function of $\cos\theta$ for selected transitions. The lines are linear fits to the data from which the $F(\tau)$ values have been extracted.

Table III displays the comparison of the lifetime data for a few selected levels obtained in the present $(n, n'\gamma)$ reaction with the lifetimes deduced from the data obtained in the (γ, γ') reaction [29]. The estimated 10% uncertainty in the stopping power is not included in the quoted values from the present measurement. The level lifetimes from the (γ, γ') data have been obtained via

$$\tau_{(\gamma,\gamma')} = \frac{g(BR)^2\hbar}{I_{s,0}}\left(\pi\frac{\hbar c}{E_s}\right)^2, \qquad (3)$$

where the branching ratio to the ground state is defined as $BR = \Gamma_0/\Gamma$, with Γ_0 being the decay width to the ground state from the level of interest and Γ being the total decay width of that level. The statistical factor, g, is given by $g = (2I_s + 1)/(2I_0 + 1) = 3$ in the case of dipole excitations for even-even nuclei [29]. The scattering intensity to an excited state s, $I_{s,0}$, is calculated as

$$I_{s,0} = g\left(\pi\frac{\hbar c}{E_\gamma}\right)^2\frac{\Gamma_0^2}{\Gamma}. \qquad (4)$$

It is apparent from Table III that the lifetimes from these two measurements agree very well. Since the calculation includes

TABLE I. Levels of ^{114}Cd observed in the present measurements. We list the $F(\tau)$ values for the levels and the branching ratios and multipole mixing ratios of the transitions.

E_{lev} (keV)	J_i^π	$F(\tau)$	E_γ (keV)	E_f (keV)	J_f^π	Multipole	δ	BR
558.38(5)	2^+	0.000(21)	558.38(5)	0.00	0^+	$E2$		
1134.44(7)	0^+	0.000(18)	576.00(5)	558.38	2^+	$E2$		
1209.60(4)	2^+	0.007(10)	651.18(5)	558.38	2^+	$M1, E2$	$-1.0^{+0.1}_{-0.1}$	100.0(10)
			1209.64(5)	0.00	0^+	$E2$		31.4(4)
1283.59(6)	4^+	0.000(14)	725.22(5)	558.38	2^+	$E2$		
1305.64(7)	0^+	0.037(48)	747.20(5)	558.38	2^+	$E2$		
1364.27(5)	2^+	0.006(14)	229.91(5)	1134.44	0^+	$E2$		<8
			805.83(5)	558.38	2^+	$M1, E2$	$0.08^{+0.05}_{-0.03}$	100.0(15)
			1364.28(5)	0.00	0^+	$E2$		90.9(11)
1732.14(7)	4^+	0.041(37)	368.00(6)	1364.27	2^+	$E2$		42.9(9)
			448.61(5)	1283.59	4^+	$M1, E2$	$-1.1^{+0.2}_{-0.2}$	29.4(5)
			522.48(5)[m]	1209.60	2^+	$E2$		100(15)
			1173.74(6)	558.38	2^+	$E2$		80.5(11)
1841.81(6)	2^+	0.012(21)	477.57(6)[m]	1364.27	2^+	$M1, E2$	$-0.4^{+0.1}_{-0.1}$	22.2(3)
			536.24(6)	1305.64	0^+	$E2$		17.1(3)
			632.16(7)	1209.60	2^+	$E2, M1$	$3.6^{+4.3}_{-1.3}$	4.9(1)
			707.30(5)[m]	1134.44	0^+	$E2$		64.4(10)
			1283.37(6)	558.38	2^+	$M1, E2$	$2.4^{+0.3}_{-0.2}$	100.0(13)
			1841.91(6)[m]	0.00	0^+	$E2$		23.9(3)
1859.62(10)	0^+	0.022(13)	495.40(6)[m]	1364.27	2^+	$E2$		6.8(2)
			1301.18(6)	558.38	2^+	$E2$		100.0(13)
1864.08(8)	3^+	0.017(14)	580.46(6)	1283.59	4^+	$M1, E2$	$-0.4^{+0.1}_{-0.1}$	21.0(4)
							$-1.6^{+0.2}_{-0.2}$	
			654.43(6)	1209.60	2^+	$M1, E2$	$-4.2^{+0.3}_{-0.3}$	100.0(15)
			1305.74(6)	558.38	2^+	$M1, E2$	$-2.2^{+0.1}_{-0.1}$	94.8(14)
1931.94(7)	4^+	0.000(81)	567.59(6)[m]	1364.27	2^+	$E2$		42.1(8)
			648.37(6)[m]	1283.59	4^+	$E2$		61.5(13)
			722.30(6)	1209.60	2^+	$E2$		100.0(13)
			1373.51(8)[n]	558.38	2^+	$E2$		13.1(6)
1958.01(7)	3^-	0.05(1)	748.40(10)	1209.60	2^+	$E1$	$-0.01^{+0.03}_{-0.04}$	27.1(4)
			1399.71(10)	558.38	2^+	$E1$	$0.07^{+0.02}_{-0.02}$	100.0(4)
1990.19(21)	6^+		706.60(10)	1283.59	4^+	$E2$		
2047.90(7)	2^+	0.046(14)	683.59(6)[na]	1364.27	2^+	$E2$		3.1(1)
						$M1, E2$	$-0.5^{+0.2}_{-0.4}$	
			742.40(6)[m]	1305.64	0^+	$E2$		8.5(2)
			838.27(7)[m]	1209.60	2^+	$0.0^{+0.3}_{-0.2}$		4.6(3)
			1489.46(6)	558.38	2^+	$M1, E2$	$0.32^{+0.03}_{-0.02}$	100.0(12)
2152.12(7)	4^+	0.040(34)	288.00(5)	1864.08	3^+	$M1, E2$	$0.16^{+0.1}_{-0.1}$	18.7(9)
			310.40(8)	1841.81	2^+	$E2$		17.3(12)
			420.21(6)[m]	1732.14	4^+	$M1, E2$	$-1.2^{+0.3}_{-1.0}$	45.3(11)
			787.82(7)[n]	1364.27	2^+	$E2$		31.1(6)
			868.39(6)	1283.59	4^+	$M1, E2$	$-0.33^{+0.05}_{-0.05}$	59.8(9)
							$2.3^{+0.3}_{-0.3}$	
			942.45(6)	1209.60	2^+	$E2$		100.0(13)
			1593.70(7)[n]	558.38	2^+	$E2$		32.2(6)
2204.30(8)	3^+	0.032(15)	472.7(5)	1732.14	4^+	$M1, E2$	$0.28^{+0.29}_{-0.20}$	
			840.09(6)	1364.27	2^+	$M1, E2$	$-0.35^{+0.13}_{-0.18}$	45.0(16)
							$-1.6^{+0.5}_{-0.5}$	
			920.64(6)	1283.59	4^+	$M1, E2$	$-2.1^{+0.2}_{-0.2}$	74.4(10)
			994.73(6)	1209.60	2^+	$M1, E2$	$-1.2^{+0.1}_{-0.1}$	75.8(10)
							$-0.53^{+0.04}_{-0.06}$	
			1645.99(6)	558.38	2^+	$M1, E2$	$-0.42^{+0.04}_{-0.05}$	100.0(12)

TABLE I. *(Continued.)*

E_{lev} (keV)	J_i^π	$F(\tau)$	E_γ (keV)	E_f (keV)	J_f^π	Multipole	δ	BR
2218.82(12)	2^+	0.238(15)	854.60(30)	1364.27	2^+	$M1, E2$	$0.6^{+1.1}_{-0.5}$	0.9(1)
			1660.34(6)	558.38	2^+	$M1, E2$	$0.19^{+0.04}_{-0.05}$	100.0(2)
			2218.82(10)	0.00	0^+	$E2$		3.1(2)
2298.67(13)	5^-	0.00(2)	340.80(10)	1958.01	3^-	$M1, E2$	<7.9	4.0(5)
			1015.2(10)[m]	1283.59	4^+	$E1$	$-0.01^{+0.01}_{-0.02}$	100.0(5)
2384.64(11)	3^-	0.05(1)	426.50(10)	1958.01	3^-	$M1, E2$	$1.2^{+0.3}_{-0.3}$	9.8(3)
							$0.1^{+0.1}_{-0.1}$	
			1175.11(10)	1209.60	2^+	$E1$	$0.01^{+0.1}_{-0.1}$	6.9(12)
			1826.32(10)	558.38	2^+	$E1$	$0.01^{+0.01}_{-0.02}$	100.0(12)
2391.20(16)	4^+	0.128(13)	1107.62(7)	1283.59	4^+	$M1, E2$	$-0.01^{+0.04}_{-0.04}$	
2400(1)	6^+		668(1)[m]	1732.14	4^+	$E2$		
2412(1)	6^+		113.9(1)	2298.67	5^-	$E1$		
2437.56(14)	0^+	0.010(20)	1879.05(7)	558.38	2^+	$E2$		
2456.35(16)	1^-	0.44(1)	2456.03(10)	0.00	0^+	$E1$		
2460.53(12)	4^-	<0.04	256.20(10)	2204.30	3^+	$E1$	$0.07^{+0.12}_{-0.12}$	9.9(7)
			502.67(10)	1958.01	3^-	$M1, E2$	$2.5^{+0.6}_{-0.5}$	18.6(7)
							$0.58^{+0.15}_{-0.11}$	
			596.30(10)	1864.08	3^++bg		$-0.02^{+0.01}_{-0.06}$	92.3(46)
			728.60(10)	1732.14	4^+	$E1$	$-0.09^{+0.14}_{-0.12}$	20.0(7)
			1176.91(10)	1283.59	4^+	$E1$	$-0.02^{+0.07}_{-0.06}$	100.0(19)
2502.6(1)	(4)	0.156(26)	1219.62(8)	1283.59	4^+			
2525.1(1)	(3)	0.018(21)	1966.70(8)	558.38	2^+			
2525.27(9)	2^+	0.039(41)	567.33(10)[m]	1958.01	3^-			
			665.47(30)	1859.62	0^+	$E2$		0.084(5)
			1160.94(8)	1364.27	2^+	$M1, E2$	$-0.34^{+0.07}_{-0.07}$	46.6(9)
			1315.55(8)	1209.60	2^+	$M1, E2$	0.65^{+18}_{-14}	100.0(13)
			2525.28(9)	0.00	0^+	$E2$		40.6(31)
2535.74(14)	5^-	0.133(77)	237.17(6)[m]	2298.67	5^-			100(30)
			803.6(8)[na]	1732.14	4^+	$E1$	$0.08^{+0.09}_{-0.10}$	51(4)
			1251.99(8)[na]	1283.59	4^+	$E1$		18(1)
2553.88(13)	0^+	0.082(22)	1189.49(9)[na]	1364.27	2^+	$E2$		18.0(8)
			1995.59(8)	558.38	2^+	$E2$		100.0(25)
2580.31(11)	2^-	0.06(1)	532.30(10)	2047.90	2^+	$E1$	$0.07^{+0.27}_{-0.18}$	6.3(4)
			622.30(10)	1958.01	3^-	$M1, E2$	$1.2^{+1.3}_{-0.6}$	5.3(4)
			1370.71(10)	1209.60	2^+	$E1$	$0.01^{+0.03}_{-0.03}$	100.0(4)
			2021.92(10)[m]	558.38	2^+	$E1$	$0.12^{+0.07}_{-0.06}$	16.5(4)
2636.33(10)	0^+	0.100(18)	1426.61(10)	1209.60	2^+	$E2$		12.1(5)
			2078.02(8)	558.38	2^+	$E2$		100.0(30)
2649.98(13)	2^+	0.063(15)	1285.53(8)	1364.27	2^+	$M1, E2$	$0.03^{+0.06}_{-0.06}$	38.1(6)
			1344.59(9)[m]	1305.64	0^+	$E2$		12.1(5)
			2649.93(23)	0.00	0^+	$E2$		100.0(93)
2660.75(17)	3^+	0.565(18)	2102.37(8)	558.38	2^+	$M1, E2$	$0.41^{+0.02}_{-0.03}$	100.0
	2^+						$1.9^{+0.1}_{-0.1}$	
2698(1)			2139.32(15)	558.38	2^+			
2700.81(11)	3^+	0.084(21)	495.40(6)[m]	2204.30	3^+	$M1, E2$		26.1(27)
			742.44(6)[m]	1958.01	3^-	$E1$		80.1(15)
							$2.6^{+1.3}_{-0.8}$	
			1417.07(9)	1283.59	4^+	$M1, E2$	$0.54^{+0.21}_{-0.13}$	19.2(7)
							$2.6^{+1.3}_{-0.8}$	
			1491.36(10)	1209.60	2^+	$M1, E2$	$0.17^{+0.24}_{-0.20}$	58.5(27)

TABLE I. *(Continued.)*

E_{lev} (keV)	J_i^π	$F(\tau)$	E_γ (keV)	E_f (keV)	J_f^π	Multipole	δ	BR
							$E2$	
			2142.46(8)	558.38	2^+	$M1, E2$	$0.51^{+0.04}_{-0.04}$	100.0(36)
							$2.9^{+0.5}_{-0.4}$	
2747.2(1)	(5)	0.000(73)	1463.59(9)	1283.59	4^+			
2749.45(12)	2^+	0.289(27)	791.46(9)[n]	1958.01	3^-	$E1$		18(1)
			1540.08(13)[n]	1209.60	2^+	$M1, E2$	$-1.9^{+1.2}_{-7.2}$	5.4(3)
			2190.93(9)	558.38	2^+	$M1, E2$	$0.11^{+0.05}_{-0.05}$	100.0(40)
							$1.8^{+0.2}_{-0.2}$	
			2749.44(20)	0.00	0^+	$E2$		5.0(8)
2756.80(12)	4	0.053(31)	798.76(10)	1958.01	3^-			38.2(28)
			1024.68(9)	1732.14	4^+			52.0(12)
			1473.22(9)	1283.77	4^+			100.0(17)
2767.50(13)	1^-	0.514(23)	2209.17(9)	558.38	2^+	$E1$		55(3)
			2767.44(9)	0.00	0^+	$E1$		100(11)
2784.23(14)	5^-	0.042(26)	1052.17(9)	1283.59	4^+	$M1, E2$		54(2)
			1500.59(9)	1732.14	4^+	$M1, E2$		100(2)
2788.73(11)	2^+	0.103(16)	1579.61(10)	1209.60	2^+	$M1, E2$	$-1.5^{+0.6}_{-1.3}$	13(1)
			2230.17(8)	558.38	2^+	$M1, E2$	$7.6^{+3.0}_{-1.9}$	100(4)
							$-0.28^{+0.04}_{-0.04}$	
2799.93(11)	1^+	0.593(29)	1590.20(10)[n]	1209.60	2^+	$M1, E2$	<0.24	19(1)
			2241.62(10)	558.38	2^+	$M1, E2$	$1.3^{+62}_{-1.0}$	25(1)
			2799.97(8)	0.00	0^+	$M1$		100(11)
2806.53(12)	3^+	0.194(21)	1522.86(9)	1283.59	4^+	$M1, E2$	$8.3^{+7.6}_{-2.6}$	86(2)
			2248.22(9)	558.38	2^+	$M1, E2$	$0.34^{+0.04}_{-0.04}$	100(5)
2811.6(2)	4^+	0.000(97)	880.8(2)	1931.94	4^+	$E2$		
			1447.74(10)	1364.27	2^+	$E2$		100(7)
			1601.96(10)	1209.60	2^+	$E2$		35(2)
2811.76(10)	2^+	0.073(27)	853.91(8)	1958.01	3^-			18(1)
			2253.48(10)	558.38	2^+	$M1, E2$	$-0.11^{+0.04}_{-0.04}$	100(5)
							$3.36^{+0.53}_{-0.44}$	
			2811.33(10)	0.00	0^+	$E2$		65(8)
2820.08(9)	4^+	0.006(82)	601.35(10)	2218.82	2^+			
			772.20(10)	2047.90	2^+			100(18)
			861.92(10)	1958.01	3^-			86(5)
2827.86(18)[n]		0.069(36)	1618.25(9)[na]	1209.60	2^+	$E2$		100.0(18)
2871.60(14)[n]	2,3	0.186(18)	913.57(9)[na]	1958.01	3^-			13(1)
			2313.24(9)[na]	558.38	2^+			100(5)
2874.43(13)[n]	2,4	0.018(27)	826.11(8)[n]	2047.90	2^+			100(2)
			916.27(9)[n]	1958.01	3^-			19(1)
			1664.77(9)[n]	1209.60	2^+			33(1)
			2316.2(2)[n]	558.38	2^+			
2880.6(1)	4,3	0.210(29)	1596.94(9)	1283.59	2^+			
2910.34(31)[n]	4	0.036(29)	707.30(5)[m]	2204.30	3^+			
			2351.96(15)	558.38	2^+			
2918.4(1)[n]	3	0.288(41)	1634.83(9)[n]	1283.59	4^+	$M1, E2$		
2932.95(21)[n]	4^+	0.187(23)	1649.35(9)[n]	1283.59	4^+	$E2$		
2936.13(9)	2^+	0.048(32)	1629.36(10)	1305.64	0^+	$E2$		56(1)
			1652.53(9)	1283.59	4^+	$E2$		100(2)
			1725.78(20)	1209.60	2^+	$M1, E2$	$-1.5^{+0.06}_{-1.4}$	85(3)
			2377.67(9)	558.38	2^+	$M1, E2$	$1.5^{+0.3}_{-0.3}$	93(6)
							$0.20^{+0.11}_{-0.07}$	
2941.0(12)	$2,3^+$	0.106(33)	1731.59(9)[n]	1209.60	2^+	$M1, E2$	$-0.9^{+0.2}_{-3.8}$	100(2)
			2382.90(9)[na]	558.38	2^+	$M1, E2$	$0.18^{+0.03}_{-0.03}$	96(6)

TABLE I. *(Continued.)*

E_{lev} (keV)	J_i^π	$F(\tau)$	E_γ (keV)	E_f (keV)	J_f^π	Multipole	δ	BR
2952.96(15)	3^+	0.316(28)	495.40(6)[m]	2456.35	1^-			
			2394.59(9)	558.38	2^+	$M1, E2$	$0.15^{+0.04}_{-0.04}$	
						$E2$		
2955.94(21)	5	0.072(70)	1672.35(10)	1283.59	4^+			
2956.30(19)	2	0.145(18)	2397.92(9)	558.38	2^+			
2999.21(11)	$1^{(-)}$	0.542(27)	420.21(6)[m]	2580.31	2^-			
			614.25(10)	2384.64	3^-	$E2$		21(2)
			2440.78(18)	558.38	2^+	$E1$		15(1)
			2999.71(9)	0.00	0^+	$E1$		100(15)
3001.12(13)	2^+	0.165(35)	954.98(10)	2047.90	2^+	$E2/M1$	$-1.5^{+0.7}_{-2.2}$	11(3)
			3001.68(11)	0.00	0^+	$E2$		100(15)
3002(1)	4^+	0.042(37)	477.57(6)[m]	2525.27	2^+	$E2$		
			2443.22(11)	558.38	2^+	$E2$		
3025.01(21)	2,3	0.080(28)	2466.63(10)[n]	558.38	2^+			
3052(1)	(2)		1841.9(1)[m]	1209.60	2^+			
3061.44(15)[n]	2^+	0.192(26)	1197.26(12)[n]	1864.08	3^-			100(15)
			2503.12(9)[n]	558.38	2^+	$M1, E2$	$-1.5^{+0.5}_{-0.7}$	95(10)
			3062(1)[n]	0.00	0^+			
3077.54(21)	2^+	0.168(47)	1868.27(10)	1209.60	2^+	$M1, E2$	$-0.42^{+0.10}_{-0.11}$	100(2)
			2519.40(20)	558.38	2^+	$M1, E2$	$-1.5^{+0.7}_{-1.7}$	33(3)
			3077.77(20)	0.00	0^+	$E2$		58(10)
3108.15(16)	$1^{(-)}$	0.571(58)	1743.98(15)	1364.27	2^+	$E1$		7(1)
			1973.27(20)	1134.44	0^+	$E1$		9(1)
			2549.65(20)	558.38	2^+	$E1$		100(8)
			3108.69(20)	0.00	0^+	$E1$		30(6)
3111.64(16)	(2)		727.37(11)	2384.64	3^-	$E2$		50(6)
			1746.88(14)	1364.27	2^+	$E1$		15(2)
3116.01(15)	3,2	0.166(19)	1067.07(10)	1931.93	4^+	$E2$		86(3)
			1274.15(11)	1841.81	2^+			100(3)
			1832.19(20)	1283.59	4^+			37(2)
			2557.36(11)	558.38	2^+			91(5)
3140.31(17)	3,2	0.112(16)	1276.65(11)[na]	1864.08	3^+			46(2)
			2581.50(11)[na]	558.38	2^+			100.0(8)
3143 (1)	6		473(1)	2669	8^+.			
3157.05(20)	2	0.015(27)	2022.11(20)[m]	1134.44	0^+			
			2598.60(12)	558.38	2^+			
3167.9(2)		0.046(92)	642.67(11)[n]	2525.27	2^+			
			1802.7(1)	1364.27	4^+			
3168.28(18)	2	0.240(53)	1959.08(12)[n]	1209.60	2^+			
3176.57(16)[n]	2,3	0.112(31)	1128.04(10)[na]	2047.90	2^+			49(3)
			1311.70(12)[na]	1864.08	3^+			68(4)
			2618.17(11)[na]	558.38	2^+			100(5)
3192.14(27)	2,3	0.140(53)	1982.55(13)[n]	1209.60	2^+			
3206.10(13)	2^+	0.145(29)	986.92(13)	2218.82	2^+	$M1, E2$	$-0.06^{+0.19}_{-0.18}$	86.0(4.3)
						$E2$	$2.8^{+2.9}_{-1.1}$	
			1247.75(13)	1958.01	3^-	$E1$		62.9(2.7)
			1900.46(13)	1305.64	0^+	$E2$		100.0(4.6)
3206.10(10)	3		1274.15(11)[n]	1931.94	4^+	$E2$	$0.4^{+0.1}_{-0.1}$	100.0(18)
			1923.14(12)[n]	1283.59	4^+	$E2$	$0.7^{+0.3}_{-0.2}$	34.7(13)
3212.97(29)	1	0.420(28)	3212.97(21)[na]	0.00	0^+			
3218.35(24)	$1^{(-)}$	0.467(27)	2659.82(20)	558.38	2^+	$(E1)$		100(9.5)
			3218.61(20)	0.00	0^+	$(E1)$		71.5(13.4)
3221.42(33)	1	0.035(91)	1915.78(16)[n]	1305.64	0^+			
3222.71(29)	0	0.170(58)	2013.12(14)[n]	1209.60	2^+			
3232.38(21)[n]	1,2,3	0.193(26)	2673.99(11)[na]	558.38	2^+			
3249.13(21)[n]	1	0.314(100)	811.15(13)[n]	2437.56	0^+			100(20)

TABLE I. *(Continued.)*

E_{lev} (keV)	J_i^π	$F(\tau)$	E_γ (keV)	E_f (keV)	J_f^π	Multipole	δ	BR
			2040.06(14)[n]	1209.60	2^+			72(8)
3257.36(14)	1,2	0.180(50)	802.10(30)[na]	2456.35	1^-			
			2047.55(13)[na]	1209.60	2^+			60(3)
			2699.14(14)	558.38	2^+			100(19)
3261.93(27)[n]	1,2,3	0.104(79)	2703.54(13)[na]	558.38	2^+			
3265.33(27)[n]	1,2	0.000(99)	2706.94(13)[na]	558.38	2^+			
3285.04(23)	$2,3^+$	0.193(32)	2001.46(11)[n]	1283.59	4^+			
3296.53(21)[n]		0.000(375)	1092.43(12)[n]	2204.30	3^+			71(4)
			2737.68(18)[n]	558.38	2^+			100(28)
3298.74(19)[n]	2,3	0.412(53)	2740.10(12)[na]	558.38	2^+			
3322.25(16)[n]	1	0.135(62)	865.35(11)	2456.35	1^-			
			2764.51(12)	558.38	2^+			100(12.4)
			3322.24(13)	0.00	0^+			68.9(14.4)
3334.31(17)[n]	2,3,4	0.200(42)	753.76(13)[na]	2580.31	2^-			
			2124.92(14)[na]	1209.60	2^+			67(3)
			2775.97(13)[na]	558.38	2^+			100(12)
3349.62(24)	2,3	0.032(84)	2792.26(18)[na]	558.38	2^+			100(13)
3366.75(31)	3	0.000(122)	2808.37(15)[n]	558.38	2^+			
3369.66(19)		0.073(27)	2811.28(9)[m,n]	558.38	2^+			
3381.91(26)	1,2,3	0.246(171)	2172.19(15)	1209.60	2^+			100(23)
			2823.81(23)	558.38	2^+			68(14)
3409.63(21)	1,2		1545.50(15)[n]	1864.08	3^+			100
			3410(1)	0.00	0^+			
3462.18(39)			3462.18(19)	0.00	0^+			
3478.48(37)			2114.21(18)[n]	1364.27	2^+			
3488.73(45)[n]			3488.73(22)[n]	0.00	0^+			
3500.17(41)			3500.17(20)[n]	0.00	0^+			
3503.78(25)			1545.50(15)[n]	1958.01	3^-			
			2198.63(20)[n]	1305.64	0^+			
3543.70(45)[n]			2985.31(22)[n]	558.38	2^+			
3552.10(49)[n]			2993.71(24)[n]	558.38	2^+			
3610.57(53)[n]			3610.57(26)[n]	0.00	0^+			

[m]This γ ray has multiple thresholds.
[n]The γ ray or level is newly observed.
[na]The γ ray is newly assigned in this work.

the branching ratio of the selected transition, it indicates that an accurate level and decay scheme must be in place.

III. DISCUSSION

In the present study, the nucleus ^{114}Cd is excited through the nonselective $(n, n'\gamma)$ reaction to achieve a comprehensive level scheme at low excitation energy and low spin. The goal is to characterize the levels up to the pairing gap (at approximately 2.5 MeV) and above, if possible, on the basis of their phonon and intruder characteristics. Figure 5 presents all levels in ^{114}Cd up to 2.5 MeV with suggested assignments. The 1^+ mixed-symmetry state is also included in the figure.

A. Intruder states and two-phonon excitations in ^{114}Cd

The origin of the second and third 0^+ states in the even-even Cd nuclei has received considerable attention. The main controversy is in assigning them to the intruder structure or to the two-phonon triplet. A good handle in removing this ambiguity is the strength of electric monopole transition, which directly provides a measure of the change in deformation corresponding to different configurations [30]. The $E0$ distributions in ^{114}Cd measured by Mheemeed *et al.* [12] support the assignment of the 0_3^+ state as the two-phonon state and the 0_2^+ state to the intruder structure. However, why the two-phonon 0_3^+ state does not decay strongly to the one-phonon 2_1^+ state, whereas the intruder 0_2^+ state does decay strongly to this state, has yet to be resolved. It is believed that two-nucleon transfer reactions give direct evidence for pairing excitations resulting in intruder states in the nuclei. Kadi *et al.* [11] assigned the 0_2^+ state in ^{112}Cd as the intruder state by considering the strong population of this state in the ^{110}Pd(^{3}He, n)^{112}Cd reaction [31]. The decay systematics over the chain of Cd isotopes [11] support the intruder origin of the 0_2^+ state in ^{114}Cd. Unfortunately, owing to the nonexistence of a stable Pd target, two-proton transfer reaction studies and direct identification of the intruder states are not possible for ^{114}Cd. The two-neutron transfer data obtained in the ^{112}Cd(t, p)^{114}Cd reaction [5], however, support the intruder assignment for the

TABLE II. Decay properties of levels in ^{114}Cd extracted from the data presented in Table I.

E_{lev} (keV)	τ (fs)	E_γ (keV)	E_f (keV)	$J_i^\pi \to J_f^\pi$	$B(E2; J_i^\pi \to J_f^\pi)$ (W.u.)	$B(M1; J_i^\pi \to J_f^\pi)$ (μ_N^2)	$B(E1; J_i^\pi \to J_f^\pi)$ (mW.u.)
0.00							
558.38(5)	147001[d]	558.38(5)	0.00	$2^+ \to 0^+$	31		
1134.44(7)	142801[d]	576.00(6)	558.38	$0^+ \to 2^+$	27.5		
1209.60(4)	44721[d]	651.18(5)	558.38	$2^+ \to 2^+$	20.3	1.6×10^{-2}	
		1209.64(5)	0.00	$2^+ \to 0^+$	0.5		
1283.59(6)	20051[d]	725.22(5)	558.38	$4^+ \to 2^+$	61.9		
1305.64(7)	$6.8 \times 10^6$1[d]	747.20(5)	558.38	$0^+ \to 2^+$	0.0026		
1364.27(5)	75021[d]	229.91(5)	1134.44	$2^+ \to 0^+$	<190		
		805.83(5)	558.38	$2^+ \to 2^+$	0.03	7.2×10^{-3}	
		1364.28(5)	0.00	$2^+ \to 0^+$	0.3		
1732.14(7)	69251[d]	368.00(6)	1364.27	$4^+ \to 2^+$	85.1		
		448.61(5)	1283.59	$4^+ \to 4^+$	11.4	4.3×10^{-3}	
		522.48(5)	1209.60	$4^+ \to 2^+$	34.0		
		1173.74(6)	558.38	$4^+ \to 2^+$	0.6		
1841.81(6)	>1200	477.57(6)	1364.27	$2^+ \to 2^+$	<11.8	$<3.2 \times 10^{-2}$	
		536.24(6)	1305.64	$2^+ \to 0^+$	<31.3		
		632.16(7)	1209.60	$2^+ \to 2^+$	<3.8		
		707.30(5)	1134.44	$2^+ \to 0^+$	<37.6		
		1283.37(6)	558.38	$2^+ \to 2^+$	<2.08	1.3×10^{-3}	
		1841.91(6)	0.00	$2^+ \to 0^+$	$<9.2 \times 10^{-2}$		
1859.62(10)	>1050	495.40(6)	1364.27	$0^+ \to 2^+$	<50		
		1301.18(6)	558.38	$0^+ \to 2^+$	<6		
1864.08(8)	>1250	580.46(6)	1283.59	$3^+ \to 4^+$	<6.1	$<2.0 \times 10^{-2}$	
					<23.1	$<7.4 \times 10^{-3}$	
		654.43(6)	1209.60	$3^+ \to 2^+$	<72.2	$<4.1 \times 10^{-3}$	
		1305.74(6)	558.38	$3^+ \to 2^+$	<1.9	$<1.5 \times 10^{-3}$	
1931.94(7)	>450	567.59(6)	1364.27	$4^+ \to 2^+$	<185		
		648.37(6)	1283.59	$4^+ \to 4^+$	<146	$<1.4 \times 10^{-3}$	
		722.30(6)	1209.60	$4^+ \to 2^+$	<132		
		1373.51(8)	558.38	$4^+ \to 2^+$	<0.7		
1958.01(7)	860^{+210}_{-140}	748.40(10)	1209.60	$3^- \to 2^+$			0.25(5)
		1399.71(10)	558.38	$3^- \to 2^+$			0.14(3)
2047.90(7)	820^{+360}_{-200}	683.59(6)	1364.27	$2^+ \to 2^+$	$5.4^{+2.0}_{-2.0}$		
					$1.1^{+1.7}_{-0.8}$	$0.003^{+0.001}_{-0.001}$	
		742.44(6)[m]	1305.64	$2^+ \to 0^+$	$10.0^{+3.3}_{-3.0}$		
		838.27(7)	1209.60	$2^+ \to 2^+$	$2.5^{++1.6}_{-1.4}$	$\leqslant 0.003$	
					$2.9^{+1.2}_{-3.0}$	$0.005^{+0.002}_{-0.002}$	
		1489.46(6)	558.38	$2^+ \to 2^+$	$0.33^{+0.17}_{-0.14}$	$0.017^{+0.005}_{-0.005}$	
2152.12(7)	>500	288.00(5)	1864.08	$4^+ \to 3^+$	<34.3	<0.26	
		310.40(8)	1841.81	$4^+ \to 2^+$	<990		
		420.21(6)	1732.14	$4^+ \to 4^+$	<335	$<9.7 \times 10^{-2}$	
		787.82(7)	1364.27	$4^+ \to 2^+$	<20		
		868.39(6)	1283.59	$4^+ \to 4^+$	<1.9	$<3.1 \times 10^{-2}$	
					<16.7	$<5.7 \times 10^{-3}$	
		942.45(6)	1209.60	$4^+ \to 2^+$	<22		
		1593.70(7)	558.38	$4^+ \to 2^+$	<0.5		
2204.30(8)	>800	472.70(5)	1732.14	$3^+ \to 4^+$	<9.2	$<5.8 \times 10^{-2}$	
		840.09(6)	1364.27	$3^+ \to 2^+$	<1.2	$<1.6 \times 10^{-2}$	
					<7.8	$<5.1 \times 10^{-3}$	
		920.64(6)	1283.59	$3^+ \to 4^+$	<8.6	$<3.7 \times 10^{-3}$	
		994.73(6)	1209.60	$3^+ \to 2^+$	<4.4	$<6.5 \times 10^{-3}$	
					<1.6	$<1.3 \times 10^{-2}$	
		1645.99(6)	558.38	$3^+ \to 2^+$	<0.12	$<4.1 \times 10^{-3}$	
2218.82(12)	129^{+12}_{-10}	854.20(10)	1364.27	$2^+ \to 2^+$	$1.2^{+2.3}_{-1.1}$	$0.005^{+0.003}_{-0.003}$	

TABLE II. *(Continued.)*

E_{lev} (keV)	τ (fs)	E_γ (keV)	E_f (keV)	$J_i^\pi \to J_f^\pi$	$B(E2; J_i^\pi \to J_f^\pi)$ (W.u.)	$B(M1; J_i^\pi \to J_f^\pi)$ (μ_N^2)	$B(E1; J_i^\pi \to J_f^\pi)$ (mW.u.)
		1660.31(10)	558.38	$2^+ \to 2^+$	$0.50^{+0.26}_{-0.24}$	$0.089^{+0.009}_{-0.009}$	
		2218.82(10)	0.00	$2^+ \to 0^+$	$0.107^{+0.017}_{-0.017}$		
2298.67(13)	>1500	340.80(10)	1958.01	$5^- \to 3^-$	<116		
		1015.2(10)	1283.59	$5^- \to 4^+$+bg			<0.22
2384.64(11)	800^{+230}_{-150}	426.50(10)	1958.01	$3_2^- \to 3_1^-$	92^{+47}_{-41}		
					$1.3^{+9.5}_{-1.3}$		
		1175.11(10)	1209.60	$3^- \to 2^+$			0.06(2)
		1826.32(10)	558.38	$3^- \to 2^+$			$0.06^{+0.02}_{-0.01}$
2391.20(16)	270^{+35}_{-30}	1107.62(7)	1283.59	$4^+ \to 4^+$	<0.13	$0.16^{+0.02}_{-0.02}$	
2437.56(14)	>1300	1879.05(7)	558.38	$0^+ \to 2^+$	<1.0		
2456.35(16)	56^{+6}_{-6}	2456.03(10)	0.00	$1^- \to 0^+$			0.05(3)
2460.53(12)	>977	256.20(10)	2204.30	$4^- \to 3^+$			<1.0
		502.67(10)	1958.01	$4^- \to 3^-$	<53		
					<15		
		596.30(10)	1864.08	$4^- \to 3^+$+bg			<0.77
		728.60(10)	1732.14	$4^- \to 4^+$			<0.09
		1176.91(10)	1283.59	$4^- \to 4^+$			<0.11
2502.6(1)	220^{+50}_{-40}	1219.62(8)	1283.59	$2^+ \to 4^+$	$43.1^{+9.0}_{-9.0}$		
2525.27(9)	>500	567.33(10)	1958.01	$2^+ \to 3^-$			
		665.47(30)	1859.62	$2^+ \to 0^+$	<5.6		
		1160.94(8)	1364.27	$2^+ \to 2^+$	<0.6	$<1.6 \times 10^{-2}$	
		1315.55(8)	1209.60	$2^+ \to 2^+$	<2.0	$<1.9 \times 10^{-2}$	
		2525.25(8)	0.00	$2^+ \to 0^+$	<0.1		
2535.74(14)	260^{+400}_{-110}	237.17(6)	2298.67	$(5^-) \to 5^-$			
		803.6(8)	1732.14	$(5^-) \to 4^+$			<0.3
		1251.92(30)[d]	1283.59	$(5^-) \to 4^+$			<0.51
2553.88(13)	460^{+175}_{-100}	1189.49(9)	1364.27	$0^+ \to 2^+$	$3.5^{+1.0}_{-1.0}$		
		1995.59(8)	558.38	$0^+ \to 2^+$	$1.5^{+0.4}_{-0.4}$		
2580.31(11)	610^{+130}_{-90}	532.30(10)	2047.90	$2^- \to 2^+$			$0.22^{+0.06}_{-0.07}$
		622.30(10)	1958.01	$2^- \to 3^-$	$10.5^{+8.6}_{-6.7}$		
		1370.71(10)	1209.60	$2^- \to 2^+$			0.21(4)
		2021.92(10)	558.38	$2^- \to 2^+$			0.011(2)
2636.33(10)	360^{+85}_{-60}	1426.61(10)	1209.60	$0^+ \to 2^+$	$1.3^{+0.2}_{-0.2}$		
		2078.02(8)	558.38	$0^+ \to 2^+$	$1.6^{+0.2}_{-0.2}$		
2649.98(13)	590^{+190}_{-120}	1285.53(8)	1364.27	$2^+ \to 2^+$	<0.05	$1.2^{+0.4}_{-0.4} \times 10^{-2}$	
		1344.59(9)	1305.64	$2^+ \to 0^+$	$0.8^{+0.2}_{-0.2}$		
		2649.93(23)	0.00	$2^+ \to 0^+$	$0.24^{+0.07}_{-0.06}$		
2660.75(17)	32^{+2}_{-2}	2102.37(8)	558.38	$3^+ \to 2^+$	$2.7^{+0.5}_{-0.5}$	$0.16^{+0.01}_{-0.01}$	
				$2^+ \to 2^+$	$14.8^{+1.5}_{-1.3}$	$4.2^{+0.8}_{-0.7} \times 10^{-2}$	
2700.81(11)	450^{+160}_{-100}	495.40(6)	2204.30	$3^+ \to 3^+$			
		742.44(6)	1958.01	$3^+ \to 3^-$			
		1417.07(9)	1283.59	$3^+ \to 4^+$	$0.5^{+0.5}_{-0.3}$	$7.6^{+3.6}_{-3.1} \times 10^{-3}$	
					$1.9^{+0.8}_{-0.7}$	$1.2^{+2.0}_{-0.8} \times 10^{-3}$	
		1491.36(10)	1209.60	$3^+ \to 2^+$	$0.05^{+0.21}_{-0.04}$	$7.76^{+2.96}_{-2.94} \times 10^{-3}$	
					$1.57^{+0.54}_{-0.51}$		
		2142.46(8)	558.38	$3^+ \to 2^+$	$0.10^{+0.06}_{-0.04}$	$3.45^{+1.37}_{-1.12} \times 10^{-3}$	
2749.45(12)	100^{+15}_{-10}	791.46(9)	1958.01	$2^+ \to 3^-$			$1.2^{+0.2}_{-0.1}$
					$0.38^{+0.14}_{-0.12}$		
		1540.08(13)	1209.60	$2^+ \to 2^+$	$1.1^{+0.5}_{-0.8}$	$0.001^{+0.005}_{-0.001}$	

TABLE II. *(Continued.)*

E_{lev} (keV)	τ (fs)	E_γ (keV)	E_f (keV)	$J_i^\pi \to J_f^\pi$	$B(E2; J_i^\pi \to J_f^\pi)$ (W.u.)	$B(M1; J_i^\pi \to J_f^\pi)$ (μ_N^2)	$B(E1; J_i^\pi \to J_f^\pi)$ (mW.u.)
		2190.93(9)	558.38	$2^+ \to 2^+$	$3.4^{+0.6}_{-0.6}$		
					$0.02^{+0.06}_{-0.02}$	$0.05^{+0.005}_{-0.006}$	
		2749.44(20)	0.00	$2^+ \to 0^+$	$0.06^{+0.01}_{-0.01}$		
2756.80(12)	730^{+1050}_{-280}						
2767.50(13)	43^{+4}_{-4}	2209.17(9)	558.38	$1^- \to 2^+$			0.32(3)
		2767.44(9)	0.00	$1^- \to 0^+$			0.29(3)
2788.73(11)	360^{+75}_{-55}	1579.79(10)	1209.60	$2^+ \to 2^+$	$0.58^{+0.33}_{-0.28}$	$1.50^{+1.76}_{-1.03} \times 10^{-3}$	
		2230.17(8)	558.38	$2^+ \to 2^+$	$1.13^{+0.21}_{-0.21}$		
					$9.5^{+4.6}_{-3.7} \times 10^{-2}$	$1.2^{+0.3}_{-0.2} \times 10^{-2}$	
2799.93(11)	28^{+3}_{-3}	1590.20(10)	1209.60	$1^+ \to 2^+$	$5.5^{+4.4}_{-5.1}$	$0.02^{+0.04}_{-0.02}$	
		2241.62(10)	558.38	$1^+ \to 2^+$	$1.4^{+1.1}_{-1.2}$	<0.03	
		2799.97(8)	0.00	$1^+ \to 0^+$		$6.4^{+1.0}_{-0.8} \times 10^{-2}$	
2806.53(12)	180^{+26}_{-22}	522.86(9)	1283.59	$3^+ \to 4^+$	$7.4^{+1.4}_{-1.2}$	$5.5^{+8.4}_{-4.2} \times 10^{-4}$	
		2248.22(9)	558.38	$3^+ \to 2^+$	$0.11^{+0.04}_{-0.03}$	$0.011^{+0.002}_{-0.002}$	
2811.76(10)	520^{+330}_{-150}	853.91(8)	1958.01	$2^+ \to 3^-$			0.19(1)
		2253.48(10)	558.38	$2^+ \to 2^+$	<0.03	$5.0^{+2.0}_{-2.0} \times 10^{-3}$	
					$0.38^{+0.16}_{-0.15}$		
		2811.33(10)	0.00	$2^+ \to 0^+$	$7.4^{+4.0}_{-3.3} \times 10^{-2}$		
2827.86(18)	550^{+640}_{-200}						
2871.60(14)	180^{+25}_{-20}						
2874.43(13)	>900						
2880.6(1)	160^{+30}_{-25}						
2918.4(1)	100^{+25}_{-20}						
2932.95(21)	180^{+30}_{-25}						
2936.13(9)	>500	1629.36(10)	1305.64	$2^+ \to 0^+$	<0.73		
		1652.53(9)	1283.59	$2^+ \to 4^+$			
		1725.78(20)	1209.60	$2^+ \to 2^+$	<0.70	$<2.1 \times 10^{-3}$	
		2377.67(9)	558.38	$2^+ \to 2^+$	<0.15	$<9.3 \times 10^{-4}$	
					<0.009	$<2.8 \times 10^{-3}$	
2941.0(12)	350^{+170}_{-90}						
2952.96(15)	90^{+10}_{-10}	495.40(6)	2456.35	$3^+ \to 1^-$			
		2394.59(9)	558.38	$3^+ \to 2^+$	$7.6^{+6.3}_{-3.8} \times 10^{-2}$	$4.5^{+0.6}_{-0.5} \times 10^{-2}$	
					$3.5^{+0.4}_{-0.4}$		
2956.30(19)	240^{+40}_{-30}						
2999.21(11)	36^{+4}_{-4}	420.21(6)	2580.31	$1^- \to 2^-$			
		614.25(10)	2384.64	$1^- \to 3^-$			
		2440.78(18)	558.38	$1^- \to 2^+$			0.009(1)
		2999.71(9)	0.00	$1^- \to 0^+$			0.32(4)
3001.12(13)	210^{+70}_{-40}	954.98(10)	2047.90	$2^+ \to 2^+$	$8.95^{+8.49}_{-5.93}$		
		3001.68(11)	0.00	$2^+ \to 0^+$	$0.44^{+0.15}_{-0.15}$		
3025.01(21)	470^{+280}_{-130}						
3061.44(15)	175^{+35}_{-25}	1197.26(12)	1864.08	$2^+ \to 3^+$			
		2503.12(9)	558.38	$2^+ \to 2^+$	$0.63^{+0.31}_{-0.25}$	$4.20^{+3.61}_{-2.42} \times 10^{-3}$	
		3062(1)	0.00	$2^+ \to 0^+$			
3077.54(21)	200^{+95}_{-50}	1868.27(10)	1209.60	$2^+ \to 2^+$	$0.41^{+0.43}_{-0.24}$	$2.0^{+1.0}_{-0.8} \times 10^{-2}$	
		2519.40(20)	558.38	$2^+ \to 2^+$	$0.14^{+0.13}_{-0.09}$	$1.0^{+1.6}_{-0.8} \times 10^{-3}$	
		3077.77(20)	0.00	$2^+ \to 0^+$	$0.14^{+0.07}_{-0.04}$		
3108.15(16)	32^{+8}_{-8}	1743.98(15)	1364.27	$1^- \to 2^+$			0.12(3)
		1973.27(20)	1134.44	$1^- \to 0^+$			0.11(3)
		2549.65(20)	558.38	$1^- \to 2^+$			0.54(12)
		3108.69(20)	0.00	$1^- \to 0^+$			0.09(2)

TABLE II. *(Continued.)*

E_{lev} (keV)	τ (fs)	E_γ (keV)	E_f (keV)	$J_i^\pi \rightarrow J_f^\pi$	$B(E2; J_i^\pi \rightarrow J_f^\pi)$ (W.u.)	$B(M1; J_i^\pi \rightarrow J_f^\pi)$ (μ_N^2)	$B(E1; J_i^\pi \rightarrow J_f^\pi)$ (mW.u.)
3116.01(15)	210^{+30}_{-25}						
3140.31(28)	330^{+60}_{-50}						
3168.28(18)	130^{+50}_{-30}						
3176.57(16)	320^{+140}_{-80}						
3192.14(27)	250^{+180}_{-80}						
3206.10(15)	250^{+70}_{-50}	986.92(13)	2218.82	$2^+ \rightarrow 2^+$	$25.6^{+10.0}_{-10.0}$	$0.008^{+0.014}_{-0.006}$	
					$0.12^{+0.1}_{-0.1}$	$0.06^{+0.01}_{-0.01}$	
		1247.75(13)	1958.01	$2^+ \rightarrow 3^-$			0.09(2)
		1900.46(13)	1305.64	$2^+ \rightarrow 0^+$	$1.66^{+0.5}_{-0.3}$		
3212.97(29)	60^{+7}_{-6}						
3218.35(24)	48^{+5}_{-5}	2659.83(11)	558.38	$1^- \rightarrow 2^+$			0.27(3)
		3218.46(11)	0.00	$1^- \rightarrow 0^+$			0.11(1)
3222.71(29)	200^{+125}_{-60}						
3232.38(21)	175^{+35}_{-25}						
3249.13(21)	90^{+60}_{-30}						
3257.26(14)	190^{+90}_{-50}						
3285.04(23)	175^{+40}_{-30}						
3298.74(19)	60^{+15}_{-10}	2740.10(12)	558.38	$\rightarrow 2^+$	$1.74^{+0.78}_{-0.64}$	$0.013^{+0.011}_{-0.007}$	
3322.25(16)	260^{+250}_{-95}						
3334.31(17)	165^{+55}_{-40}						

[d]The lifetime has been taken from the NDS [36] for transition strength calculations.

0_2^+ state. Achieving a complete resolution of the ambiguity of the 0^+ states is difficult, and it has been suggested that these states might have lost their own characteristic behavior through strong mixing of their normal and intruder properties [32]. The peculiar decay pattern of these two 0^+ states can be explained by considering the constructive and destructive interference between two strong $E2$ decay amplitudes [3] corresponding to the intruder and normal configurations.

Intruder states occurring near the two-phonon triplet are well-known phenomena in near-single-closed-shell nuclei [33]. These extra states have been successfully explained as arising from two-particle, two-hole excitations across the closed shell [3]. The interacting boson model (IBM) has been found to be a powerful tool in explaining the complicated structure of these nuclei resulting from two coexisting configurations. It is a standard practice to assign the normal configuration to some dynamical symmetry limit of the IBM and the intruder configuration to another dynamical symmetry limit corresponding to a slightly more deformed shape of the nucleus. The resultant structure of the nucleus so formed is hence due to the coexistence of intruder and normal configurations. However, it is quite obvious that the ideal decay pattern of the normal and intruder states will be distorted by the interactions between these structures. It is possible that the mixing between these structures is so strong that they lose their identities. Theoretically, it is possible to have mp-mh excitations developing into more than one intruder configuration [9]; however, experimental data to support the existence of many intruder configurations is not very convincing at this moment. Hence, we shall concentrate on the intruder structure corresponding to one-proton boson excitation across the $Z = 50$ shell gap, creating three valence proton bosons, that is, a two-particle, four-hole structure, in ^{114}Cd.

TABLE III. Comparison of a few selected level lifetimes extracted from the present $(n, n'\gamma)$ measurement with those available from the (γ,γ') reaction.

E_{lev} (keV)	$\tau(n, n'\gamma)$ (fs)	$\tau(\gamma, \gamma')$ (fs)
2456.0	56^{+6}_{-6}	40 ± 10
2767.5	43^{+4}_{-4}	38 ± 9
2799.9	28^{+3}_{-3}	28 ± 7
2999.2	36^{+4}_{-4}	32 ± 9

The structure of ^{114}Cd has been successfully explained in the framework of IBM-II as a coexistence of normal and intruder bands [8,9,34]. Besides the well-known ground-state band, the authors suggested a complete intruder picture belonging to the O(6) symmetry for ^{114}Cd nucleus. Selection of O(6) symmetry is justified since the $R_{4/2}[=E_4^+/E_2^+]$ ratio for the intruder band in this nucleus is $\sim$2.6, close to the value expected for a γ-soft vibrator exhibiting O(6) dynamical symmetry in the IBM framework. Figure 6 shows the intruder band structure in ^{114}Cd, along with the similar structure of ^{110}Ru and ^{122}Ba nuclei. Each of these three nuclei has 6 valence protons and 16 neutrons. From this figure, it is clear

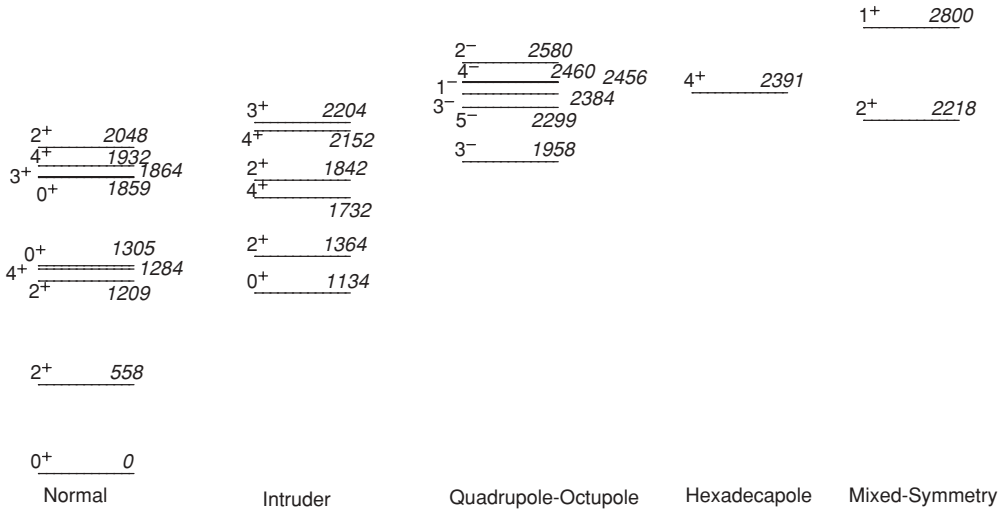

FIG. 5. Characterization of levels below 2.5 MeV in ^{114}Cd.

that the decay pattern of the intruder structure in ^{114}Cd more closely resembles the decay pattern of ^{110}Ru, exhibiting O(6) symmetry.

The intruder structure in ^{114}Cd is well known, but we have added 2^+ (1842 keV), 3^+ (2204 keV) and 4^+ (2152 keV) states to this intruder structure by comparison with ^{110}Ru. The 2^+_4 state at 1842 keV has a strong $E2$ transition to the intruder 0^+_2 state, which supports its intruder origin. A comparable $E2$ transition from this state to the normal 0^+_3 state indicates a sizable "normal" contribution in the wave function of this state. This is understandable because the origin of the 2^+_4 state may get complicated owing to the presence of nearby "normal" three-phonon 2^+ state and the first mixed-symmetry 2^+ states. All these 2^+ states have a similar quantum number, $\nu = 1$. Hence, the close proximity in excitation energy may result in strong mixing between these states and may perturb their decay patterns. The detailed structures of these 2^+ states are discussed in the following sections.

The 3^+ level near 2204 keV was observed in thermal neutron capture [12] as well as in the previous inelastic neutron scattering [35] measurements. No lifetime data are available for this level. The mean lifetime of this level is too long to be measured in the scope of the present measurement. Hence, only an upper limit (>800 fs) is obtained for the mean lifetime of this level. The expected 362-keV branch from this state to the 1842-keV state supporting its intruder origin has not been observed in the presence of high backgrounds. However, the possibility of this state belonging to the "normal" phonon structure is ruled out since the excitation energy of this state is too high to be a member of the three-phonon quintuplet and the four-phonon multiplet does not exhibit a 3^+ member. The population of this state is inhibited in the transfer and direct reactions [36], indicating that this state may be populated not as a result of single-particle or single-step processes but by multistep excitation. Strong branching from this state to both the normal as well as to the intruder states has been observed. Hence, the 3^+_2 state at 2204.5 keV is assigned as the 3^+ member of the O(6) intruder structure.

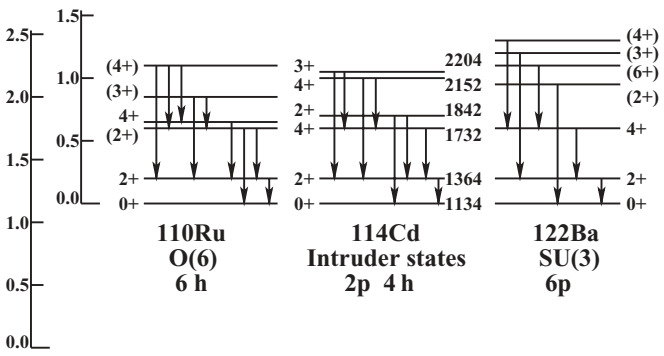

FIG. 6. Comparison of intruder states as observed in ^{114}Cd with the structures of ^{110}Ru and ^{122}Ba. Data for ^{110}Ru and ^{122}Ba are taken from the literature.

The 4^+ level at 2152 keV was observed in thermal neutron capture [12] as well as in the previous inelastic neutron scattering [35] measurements. Although the spin and parity of this level had been assigned as 4^+ in the neutron capture study, the inelastic neutron scattering data indicated the spin and parity of this state could be 2^+. We confirm the 4^+ assignment of this level. For the first time, we have also obtained an upper limit (>500 fs) for the mean lifetime of this level. The strongest branch observed from this level is to the intruder 1732-keV level. Branches have been observed to the intruder as well as to the normal states. Considering that this state is too low in excitation energy to be considered as the member of the four-phonon level and has strong $E2$ branches to the intruder states we assign this state to the intruder structure. The distortion in the decay pattern of the $E2$ decays to the "normal" phonon states can be explained as a result of mixing between the normal and intruder structures as discussed in Sec. III E.

The intensity ratios of the interband and intraband transitions for the intruder configurations are compared with those of ^{110}Ru and ^{122}Ba in Table IV. Since we have not observed the weak $3^+_\gamma \rightarrow 2^+_\gamma$ 362-keV transition in ^{114}Cd, the intensities in this case are taken from Ref. [36]. From the comparison,

TABLE IV. Comparison of the ratio of $E2$ intensities for the different decay branches in ^{114}Cd, ^{110}Ru, and ^{122}Ba nuclei. Data for ^{110}Ru and ^{122}Ba nuclei have been taken from the literature. Data for $3^+_\gamma \rightarrow 2^+_\gamma$ and $3^+_\gamma \rightarrow 2^+_{gs}$ intensities are taken from Ref. [36]

Ratios	^{110}Ru	^{114}Cd	^{122}Ba
$\frac{2^+_\gamma \rightarrow 2^+_{gs}}{2^+_\gamma \rightarrow 0^+_{gs}}$	1.1	0.3	>52.8
$\frac{3^+_\gamma \rightarrow 2^+_\gamma}{3^+_\gamma \rightarrow 2^+_{gs}}$	0.2	0.1	<0.1
$\frac{4^+_\gamma \rightarrow 4^+_{gs}}{4^+_\gamma \rightarrow 2^+_\gamma}$	0.5	2.6	0
$\frac{4^+_\gamma \rightarrow 2^+_{gs}}{4^+_\gamma \rightarrow 2^+_\gamma}$	0.2	1.8	0

it is apparent that the intruder structure in ^{114}Cd agrees more closely with the decay pattern of the respective levels in the O(6) ^{110}Ru nucleus.

Because the low-spin structure of the stable even-even Cd nuclei has been explained reasonably well in the framework of the IBM, it is useful to compare the experimental results with the predictions of the IBM calculations. In the IBM, collective motion of a nucleus is described by the excitations of the s and d bosons with angular momentum 0 and 2, respectively. This introduces a symmetry group U(6) with three dynamical symmetry limits: U(5), O(6), and SU(3). The geometrical analogs of these three limits correspond to vibrational, γ-soft, and rotational nuclei. Mixed spdf IBM-I calculations have been performed by using the code of Kusnezov [37]. The model describes states as a result of the interaction between normal and intruder configurations following U(5) and the O(6) limits of the dynamical symmetry. Details of this calculations may be found elsewhere [22]. As shown in Fig. 7, the level energies predicted by these calculations agree well with the experimental data within ~100 keV.

B. Nature of three-phonon structure in ^{114}Cd

The multiphonon interpretation of the low-energy states in ^{114}Cd nucleus was first proposed by Fahlander *et al.* [13]. Later, Casten *et al.* also suggested a quintuplet of five levels below 2 MeV as the probable candidate for the three-phonon excitations [1]. We have explored the potential of these states to be the members of the three-phonon quintuplet. Figure 8 shows a comparison of the energies of proposed three-phonon states over the chain of Cd isotopes. From these energy systematics, both the 2^+_4 and 2^+_5 states are potential candidates for three-phonon states. As pointed out by Lehmann *et al.* the decay patterns of the 2^+ three-phonon states in even-even Cd nuclei are found to be highly ambiguous [6]. For ^{112}Cd, no evidence for a pure 2^+ three-phonon state has been found. Both the 2^+_4 and 2^+_5 states at 2122 and 2156 keV in ^{112}Cd are interpreted as having large intruder contributions. Assignment as the 2^+ member of the three-phonon quintuplet is favored for the 2^+_4 state over the 2^+_5 state by considering the strong mixing resulting in the highly perturbed decay pattern of the 2^+_4 state. Similar ambiguity has been observed by Kadi *et al.* for ^{116}Cd [11]. In contrast, the 2^+_5 states at 2356 keV in ^{110}Cd and at 2486 keV in ^{108}Cd have been found to agree well with the expectations for the 2^+ member of the three-phonon quintuplet [16–18]. Aprahamian *et al.* have found that the 2^+ level at 1916 keV is quite consistent with the expectation of the three-phonon picture in ^{118}Cd [20]. Considering the ambiguous nature of the 2^+ members of the three-phonon quintuplets in the Cd nuclei, we discuss the detailed decay patterns of the 2^+_4 and 2^+_5 states in the following paragraphs.

There are two possible interpretations to explain the behavior of the low-lying states in ^{114}Cd [1,13]. It has been shown that the levels below 2.5 MeV in ^{114}Cd can be explained as a pure vibrator with extreme anharmonicity and without any intruder excitations. Though this picture explains the observed $B(E2)$ values reasonably well, some serious discrepancies were observed while explaining the excitation energies of the multiphonon states. In an alternative approach, a vibrator configuration with moderate anharmonicity is mixed with the intruder configuration. This picture explains the excitation energies of the multiphonon levels well but failed to explain all the observed $B(E2)$ values. Especially, the negligible $B(E2)$ values from the three-phonon 0^+_4 and 2^+_4 levels to the two-phonon states could not be explained. Recently, it has been found that the assignment of the 2^+_4 state at 1842 keV as a member of the three-phonon quintuplet [1] is in direct contradiction of the theoretical prediction following the

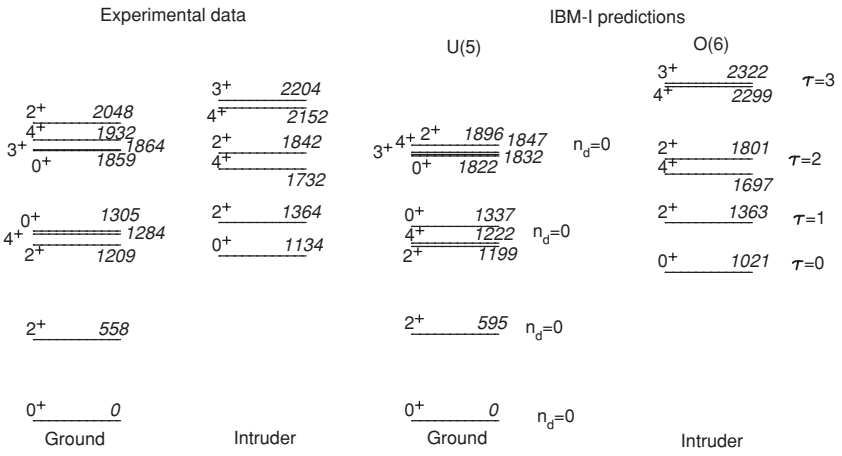

FIG. 7. Comparison of experimental level energies with the IBM1 U(5)-O(6) predictions.

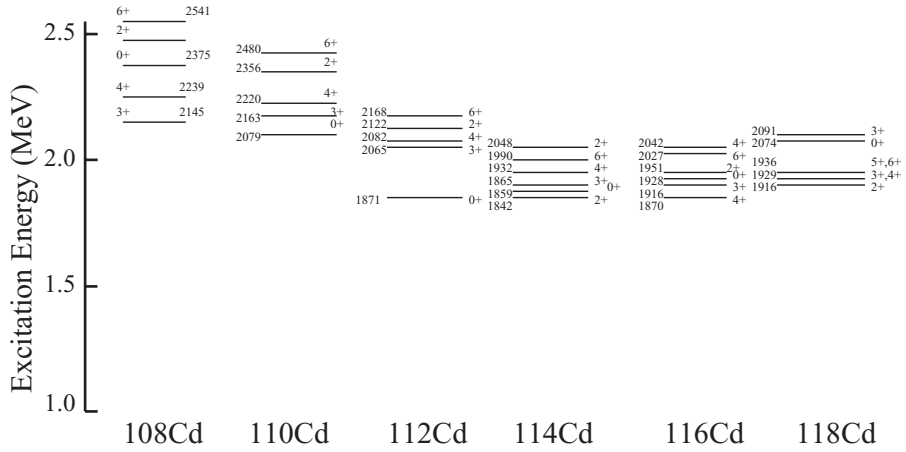

FIG. 8. Comparison of three-phonon states over the chain of even Cd isotopes.

U(5)-O(6) description of ^{114}Cd in IBM-II [34]. Further comparison with the structure of the ^{110}Ru nucleus supports the intruder origin of the 2_4^+ state in ^{114}Cd [34]. A large $E0$ branch from this state to the two-phonon 2_2^+ state at 1210 keV has been observed by Mheemeed *et al.* [12], indicating that the configuration of this state is very different from that of the normal states.

The lifetime of the 2_4^+ state has been measured by multiple Coulomb excitation [13] as well as by the GRID technique [1]. The values obtained in these two methods do not agree with each other. The lifetime of the 1842-keV state obtained with GRID is much higher ($\tau > 4.5$ ps) than the value obtained in the Coulomb excitation studies ($t_{1/2} = 0.65[12]$ ps). The limit obtained in the present measurement ($\tau > 1.2$ ps) is slightly higher than the value obtained in Coulomb excitation but much lower compared to the value obtained in the GRID technique. The disagreement between different measurements can likely be explained by considering the complexity of the feeding involved in Coulomb excitation as well as in the GRID technique. Unfortunately, a lifetime value of $\sim$1 ps is at the limit of the present $(n, n'\gamma)$ method. Hence, we present only a limit for the mean lifetime of the 2_4^+ state at 1842 keV. Branching ratios of all the transitions decaying from this level and measured in the present experiment agree well with the previous values, except for the 1842-keV transition to the ground state. Our value disagrees with the thermal neutron capture data [12] but agrees with the ^{114}Ag β-decay data [38]. The disagreement with the thermal neutron capture data could be because the 1842-keV transition is a doublet and that might not have been understood in the thermal neutron capture measurement. The 707-keV transition from the 2_4^+ state to the 0_2^+ state is also a doublet and is contaminated by the 707-keV transition from the 6^+ level at 1990 keV to the 4_1^+ state at 1284 keV. However, since the population of the 6^+ state is weak in the present measurement, the 707-keV transition is dominated by the decay from the 2_4^+ state. The observed multipole mixing ratios are found to be in excellent agreement with the previous results except for the 477-keV transition. It may be because the 477-keV transition in the present measurement is contaminated by the nearby background radiation of 477.6 keV. Strong and comparable $E2$ transitions from this state to both the 0_2^+ and 0_3^+ states have been observed in the present measurement. A considerable $E2$ branch has also been observed to the intruder 2_3^+ state at 1364 keV. Comparatively weak $E2$ branches have been observed from this state to the normal 2_2^+, 2_1^+, and 0_1^+ states.

The mean lifetime of the 2_5^+ state at 2047.9 keV is measured as 820^{+360}_{-200} fs in the present experiment, which is consistent with the measurement of Casten *et al.* following the GRID technique [1]. The branching ratios and the multipole mixing ratios also agree well with the previous measurements. The main decay branch from this level is the 1489-keV transition to the 2_1^+ state. Considering the intensity of this decay as 100%, we have calculated the detection sensitivity of our setup as $\sim$1.4%. With this sensitivity, we have not observed a 2047-keV transition from this level. The excitation function for the 2047-keV γ ray shows a much higher threshold. Hence, we have removed the assignment of the 2047-keV ground-state transition from this level. We confirm the tentative $E2$ assignment for the 742-keV transition to the 0_3^+ level at 1305 keV, which we have favored as the normal two-phonon level, therefore supporting the assignment of 2047-keV level as the member of a three-phonon quintuplet. Another 838-keV transition from this level to the two-phonon 2_2^+ level is also observed. In our previous paper [21], we assigned this level as a weak mixed-symmetry fragment. The mixed-symmetry $2_{1,\mathrm{ms}}^+$ state in ^{114}Cd has been found at 2218 keV. Since both the three-phonon 2^+ state and the $2_{1,\mathrm{ms}}^+$ state have similar quantum number ν and they are only $\sim$170 keV apart in excitation energy, this mixing is quite obvious.

Figure 9 displays the $E2$ decay pattern of the positive-parity levels in ^{114}Cd up to $J^\pi = 4^+$ and below 2.5 MeV. The thickness of the arrows represents the relative $E2$ strengths of the decay branches and the dashed lines indicate that only upper limits are available for these transitions. The mean lifetimes of the 2_1^+, 0_2^+, 2_2^+, 4_1^+, 0_3^+, 2_3^+, and 4_2^+ states are too long to be measured in the present measurement and hence have been taken from Ref. [36]. The $E2$ branches from these levels displayed in the figure are calculated by using the mixing ratios and the branching ratios obtained in the present measurement. The decay branches with upper limits are not labeled in the figure. The 2_4^+ state at 1842 keV has comparable $E2$ branches to the 0_2^+ and 0_3^+ states and considerable $E2$ strength to the intruder 2_3^+ state. The 2_5^+ state at 2048 keV

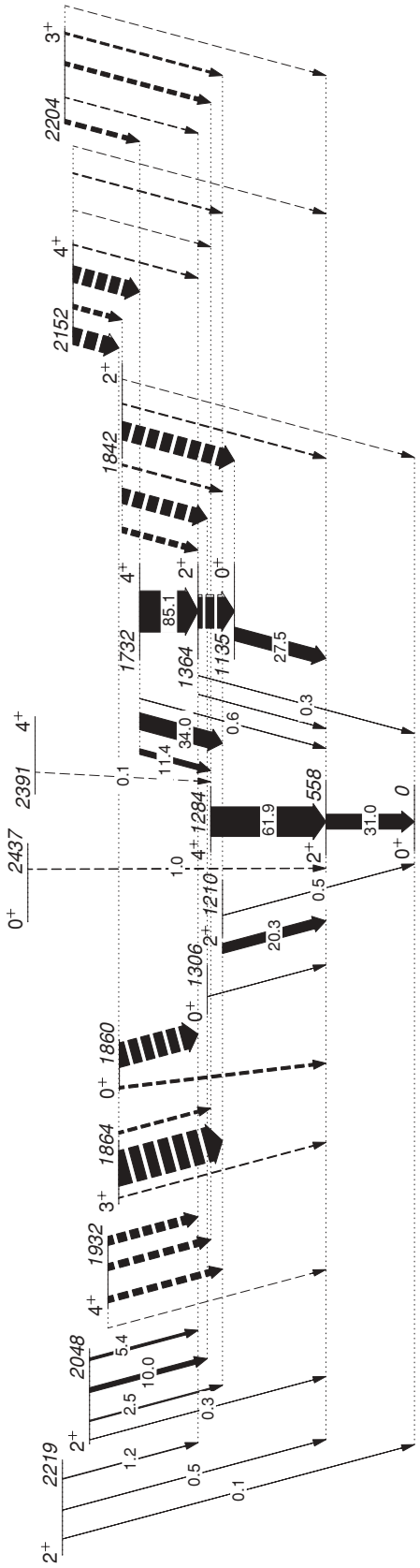

FIG. 9. Experimental results for the $E2$ decay branches from the positive-parity states below 2.5 MeV in ^{114}Cd. Dashed lines indicate the relative $B(E2)$ strengths. See text for details.

has stronger $E2$ branches to the "normal" 0_3^+ and 2_1^+ states compared to the branch to the intruder 2_3^+ state. No branch has been observed from this state to the 0_2^+ state, favored as the intruder state in the present measurement. Considering this $E2$ decay pattern, we conclude that the 2_5^+ state is favored as the member of the three-phonon state, whereas the 2_4^+ state is favored as an intruder. The mixed nature of the 2_4^+ state is discussed in more detail in Sec. III E. The 2_6^+ state at 2219 keV has weak $E2$ decay branches to the normal and intruder states and has been reported as the lowest mixed-symmetry state [21].

No suitable candidate has been found for the 0^+ member of the three-phonon multiplet. The only 0^+ state in the expected three-phonon energy range lies at 1859.6 keV. The strongest decay branch from this state is to the intruder 2_3^+ state at 1364 keV. A weak branch has been observed to the normal one-phonon 2_1^+ state at 558 keV. No transition has been observed so far from this state to the two-phonon states, contradicting its three-phonon interpretation. One reason could be that the expected 650-keV transition from this state to the two-phonon 2_2^+ state at 1209.6 keV is difficult to measure in the present experiment owing to the presence of the strong 651-keV transition from the 2_2^+ state to the 2_1^+ state. The next 0_5^+ state is observed at 2437 keV, too high to be considered as the three-phonon member. Moreover, the 0_5^+ state only weakly decays to the 2_1^+ state, excluding its phonon origin. Interestingly, a similar ambiguous behavior of the $0_{3\text{ph}}^+$ state has been observed in ^{112}Cd [19,39]. Therefore, we agree with the observation, as found for the ^{112}Cd nucleus [39], that it is difficult to explain the phonon characteristics of the lower spin states in ^{114}Cd.

We have assigned the 3_1^+ state at 1864 keV as the 3^+ member of the three-phonon quintuplet. This state was observed before in the thermal neutron capture reaction [12]. An upper limit ($\tau > 1250$ fs) for the mean lifetime of this level has been obtained in the present measurement. We have not observed two weak branches, 132- and 500-keV transitions, from this level, but the branching ratios of three other strong transitions observed in this measurement agree well with the previous study [36]. The multipole mixing ratio δ of the 654-keV transition has been obtained as $\delta = -4.2(3)$, consistent with the value of $\delta = -4.2^{+8}_{-6}$ found in the literature [12,36]. The δ value for the 1305-keV transition has been measured as $\delta = -2.2(1)$. This value agrees very well with the value obtained in the previous $(n, n'\gamma)$ measurement ($\delta = -2.20(15)$ [35]) but disagrees with the value obtained in a $\gamma - \gamma$ angular correlation measurement ($\delta = +0.19^{+22}_{-16}$) following thermal neutron capture [40]. Two values for the multipole mixing ratio have been obtained for the 580-keV transition. Considering that $M1$ nature was favored for this transition in the thermal neutron capture reaction [12], we favor the value of $\delta = -0.4(1)$. Strong $E2$ decays to the two-phonon 2_2^+ and 4_1^+ states and very weak decay to the intruder 2_3^+ state indicate that this level retains its phonon characteristics. The energy systematics and IBM-II predictions are also consistent with this assignment.

The state at 1932 keV has been observed in the previous (n, γ) reaction [12], and the spin of this state was assigned tentatively as 4^+ [36]. We confirm the 4^+ spin assignment

to this level and include this level as the 4^+ member of the three-phonon quintuplet. We provide an upper limit for the mean lifetime ($\tau > 450$ fs) of this level from the present measurement. We have observed a new transition of 1373 keV from this level to the 2_1^+ state. The branching ratios obtained for the 648- and 722-keV transitions to the respective 4_1^+ and 2_2^+ states are in very good agreement with the previous study [36]. The branching ratio for the 568-keV transition is observed to be slightly higher, which could be explained by the doublet nature of this transition. The weak 200-keV transition from this level to the 4_2^+ state is believed to be below the detection threshold. Considering strong $E2$ branches to the 2_2^+ and 4_1^+ states, we favor this state as the 4^+ member of the three-phonon quintuplet. The $E2$ branch to the intruder 2_3^+ state can be understood as a result of mixing, as discussed in Sec. III E.

C. Hexadecapole excitation in ^{114}Cd

The $K^\pi = 4^+$ states have received considerable attention, especially in the rare-earth region. Confusion arises as to the assignment of these states. Their strong population in the single-nucleon transfer reaction would indicate a bandhead of $K^\pi = 4^+\Gamma$ band, whereas the strong $E2$ transition to the 2^+ member of the γ band would imply membership in $\gamma\gamma$ excitations. The 4^+ state at 2391 keV in ^{114}Cd fits neither the normal quadrupole interpretation nor the intruder picture. The mean lifetime of this state is found as 270^{+35}_{-30} fs in the present measurement. A strong $M1$ transition of $0.16^{+0.02}_{-0.02}$ μ_N^2 to the 4_1^+ state at 1284 keV has been observed. The weak branches to the 4_2^+ and 4_3^+ states as mentioned in the literature are believed to be below our detection limit. A strong $M1$ transition to the two-phonon state suggests that this state may be the 4^+ member of the two-phonon mixed-symmetry $2_1^+ \bigotimes 2_{1,\mathrm{ms}}^+$ multiplet. In ^{114}Cd, the $2_{1,\mathrm{ms}}^+$ state has been observed at 2218 keV [21] whereas the 2_1^+ state is found at 558 keV. Hence, states originating from coupling between the 2_1^+ state and the $2_{1,\mathrm{ms}}^+$ states are expected at a sum energy of $\sim$2.8 MeV. Therefore, it is believed that the 4_1^+ state at 2391 keV is too low in energy to be a member of this quadrupole mixed-symmetry multiplet.

To explore whether the origin of this state has multiphonon nature, we considered the population intensity of this state in the inelastic scattering and single-nucleon transfer reaction. It is believed that inelastic scattering as well as the single-nucleon transfer reaction prefer to populate the one-step excited states, and the population of multistep excited states through this type of reaction gradually decreases in intensity. This state has been populated strongly in 55-MeV proton inelastic scattering reaction performed by Koike *et al.* [41], supporting its one-phonon nature. Strong population of this state has also been observed in the single-nucleon transfer reaction (d,^{3}He) [42], suggesting the origin of this state as one-phonon hexadecapole excitation.

A strong $E4$ component has been observed for the 2.22-MeV state in ^{110}Cd and 2.33-MeV state in ^{116}Cd [41]. For ^{112}Cd, the hexadecapole excitation has been found to be fragmented around 2.5 MeV [43]. These energy systematics over the chain of Cd isotope are consistent with the assignment of the 4_4^+ state at 2391 keV in ^{114}Cd as a hexadecapole excitation.

D. Isovector dipole excitation in ^{114}Cd

The observation of strong $M1$ transitions between low-lying states indicates proton-neutron antisymmetries between the wave functions. Such states, which are not fully symmetric with respect to the proton and neutron wave functions, are called mixed-symmetry states. Figure 10 displays the $M1$ branches below 3.0 MeV in ^{114}Cd observed in the present measurements. The branches weaker than 10^{-3} μ_N^2 are not displayed. Dashed lines indicate that the lifetimes for these levels are not definite and hence give the relative $M1$ strengths. A strong $M1$ transition of 0.089(9) μ_N^2 has been observed from the first excited mixed-symmetry $2_{1,\mathrm{ms}}^+$ state at 2219 keV to the 2_1^+ normal phonon state [21]. Harmonic coupling of this state with the normal isoscaler fully symmetric state ($2_1^+ \bigotimes 2_{1,\mathrm{ms}}^+$) leads to five states with $J^\pi = 0^+$ to 4^+, which are expected near the sum energy of these two states (i.e., at $\sim$2.8 MeV). Destruction of the mixed-symmetry phonon is expected to give strong $M1$ transitions from these states to the two-phonon states as well as a weak $E2$ transition from these states to the one-phonon 2_1^+ state, whereas strong $E2$ transitions from these states to the $2_{1,\mathrm{ms}}^+$ state result from the destruction of the normal phonon.

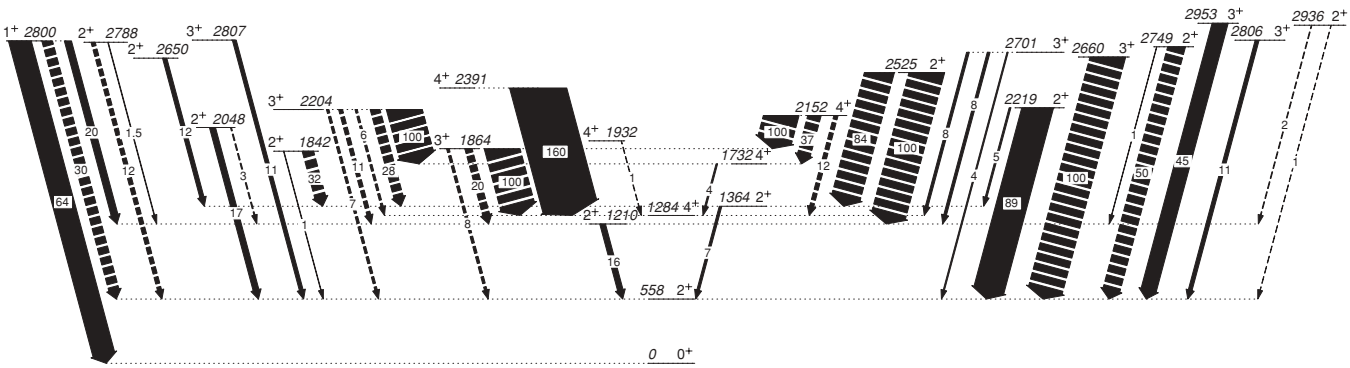

FIG. 10. Observed $M1$ branches in ^{114}Cd below 3.0 MeV. Only transitions with $B(M1)$ values greater than 0.001 μ_N^2 are shown and are labeled in units of 10^{-3} μ_N^2. Dashed lines indicate relative $B(M1)$ values.

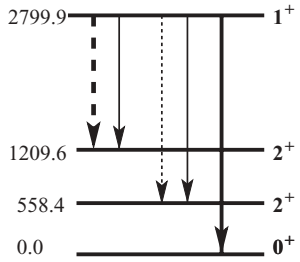

FIG. 11. Decay pattern of the probable two-phonon mixed-symmetry 1^+ state at 2800 keV. The solid lines represent $M1$ transitions whereas the dashed lines represent $E2$ transitions.

The stable Cd nuclei have been studied by Kohstall *et al.* through photon scattering to measure the isovector dipole excitations [29]. Mixed-symmetry $1^+_{\rm ms}$ states have been identified in ^{108}Cd at 3454 keV [44] and in ^{112}Cd at 2931 keV by their strong $M1$ transitions to the ground state. For ^{116}Cd this strength has been found to be fragmented over three states, with the strongest fragment at 3068 keV. For ^{110}Cd, this state has been found at 3044 keV. Hence, considering the energy systematics over the chain of Cd isotopes, the $1^+_{\rm ms}$ state is expected around 2.9 MeV excitation energy in ^{114}Cd.

The $1^+_{\rm ms}$ state can be understood as the dipole member of the $2^+_{1,\rm ms} \otimes 2^+_1$ multiplet. In nuclear resonance fluorescence, strong dipole excitation has been observed for states at 2800, 3000, and 3110 keV in ^{114}Cd [29]. The parities of the states at 3000 and 3110 keV could not be resolved in the present or previous measurements; however, from the vanishing yield of these states in the β decay of ^{114}Ag [38], we tentatively assign negative parity to these states. We confirm the 1^+ spin and parity assignment for the 2800-keV state. The mean lifetime of this state has been measured as 28^{+3}_{-3} fs in this experiment. Figure 11 shows the decay pattern of the 2800-keV state. This decay pattern is very similar to that observed for the $1^+_{\rm ms}$ state in ^{112}Cd at 2931 keV [39] but is slightly different from the decay pattern for the $1^+_{\rm ms}$ state in ^{108}Cd [45]. The expected $E2$ transition to the $2^+_{1,\rm ms}$ state at 2218 keV is not observed. The $M1$ strength of the transition to the two-phonon 2^+_2 state has been found to be $0.02^{+0.04}_{-0.02}\ \mu_N^2$ and that to the ground state is $0.064^{+0.01}_{-0.008}\ \mu_N^2$. In the vibrational U(5) limit, the $1^+_{\rm ms}$ state is expected to decay by magnetic dipole transitions dominantly to the two-phonon states, whereas the dipole transition from this state to the ground state is inhibited. This transition is possible as a result of the nonvanishing expectation value for the d-boson number in the ground state as observed for many γ-soft O(6) nuclei [46–48]. The strong $M1$ transitions from the $1^+_{\rm ms}$ state to the ground state as observed in the Cd nuclei can be explained in terms of these nuclei exhibiting both U(5) and O(6) symmetries.

E. IBM-II Calculations

Recently, efforts have been made to explain the ^{114}Cd nucleus in the framework of neutron-proton interacting boson model (IBM-II) [34]. It has been found that the low-energy structure can be explained reasonably well by considering the coexistence of normal and intruder bands. We have compared the results of the present work with IBM-II calculations similar to those of Garrett *et al.* [39]. The computer codes NPBOS and NPEM [49] were used to calculate the excitation energies of different levels and the transition strengths between them. The normal and intruder states were calculated separately using the Hamiltonian

$$\hat{H} = \epsilon(d^\dagger_\pi \tilde{d}_\pi + d^\dagger_\nu \tilde{d}_\nu) + \hat{V}_{\pi\pi} + \hat{V}_{\nu\nu} + \kappa\,\hat{Q}_\pi\,\hat{Q}_\nu + \hat{M}_{\pi\nu}. \quad (5)$$

The interaction between like bosons, $\hat{V}_{\rho\rho}$, is given by

$$\hat{V}_{\rho\rho} = \sum_{L=0,2,4} \frac{1}{2} C_{L_\rho} \sqrt{2L+1}[(d^\dagger_\rho d^\dagger_\rho)^{(L)}(\tilde{d}_\rho \tilde{d}_\rho)^{(L)}]^{(0)}. \quad (6)$$

The quadrupole-quadrupole interaction between proton and neutron bosons is represented by

$$\hat{Q}_\rho = (s^\dagger_\rho \tilde{d}_\rho + d^\dagger_\rho s_\rho)^{(2)} + \chi_\rho (d^\dagger_\rho \tilde{d}_\rho)^{(2)}, \quad (7)$$

and the Majorana interaction that acts on states that are not fully symmetric under the interchange of the proton and neutron degrees of freedom is given by

$$\hat{M}_{\pi\nu} = -\sum_{k=1,3} 2\xi_k (d^\dagger_\pi d^\dagger_\nu)^{(k)}(\tilde{d}_\pi \tilde{d}_\nu)^{(k)} + \xi_2 (d^\dagger_\pi s^\dagger_\nu - s^\dagger_\pi d^\dagger_\nu)^{(2)}(\tilde{d}_\pi s_\nu - s_\pi \tilde{d}_\nu)^{(2)}. \quad (8)$$

The two configurations calculated separately were then allowed to mix using the interaction

$$\hat{H}_{\rm mix} = \alpha(s^\dagger_\pi s^\dagger_\pi + s_\pi s_\pi)^{(0)} + \beta(d^\dagger_\pi d^\dagger_\pi + \tilde{d}_\pi \tilde{d}_\pi)^{(0)}. \quad (9)$$

An energy gap, Δ, is added to the intruder configuration to shift its energy relative to the normal ground state before diagonalization takes place. With the wave functions determined, the electromagnetic transition rates $\hat{T}(E0)$, $\hat{T}(M1)$, and $\hat{T}(E2)$ are calculated for respective $E0$, $M1$, and $E2$ transitions via

$$\hat{T}(E0) = e^{(0)}_n \left(e^{(0)}_{\pi_n} d^\dagger_{\pi_n} \tilde{d}_{\pi_n} + e^{(0)}_{\nu_n} d^\dagger_{\nu_n} \tilde{d}_{\nu_n}\right)^{(0)} + e^{(0)}_i \left(e^{(0)}_{\pi_I} d^\dagger_{\pi_I} \tilde{d}_{\pi_I} + e^{(0)}_{\nu_I} d^\dagger_{\nu_I} \tilde{d}_{\nu_I}\right)^{(0)}, \quad (10)$$

$$\hat{T}(M1) = \sqrt{\frac{30}{4\pi}} \left(g_n (g_{\pi_n} d^\dagger_{\pi_n} \tilde{d}_{\pi_n} + g_{\nu_n} d^\dagger_{\nu_n} \tilde{d}_{\nu_n})^{(1)} + g_i \left(g^{(0)}_{\pi_I} d^\dagger_{\pi_I} \tilde{d}_{\pi_I} + g_{\nu_I} d^\dagger_{\nu_I} \tilde{d}_{\nu_I}\right)^{(1)}\right), \quad (11)$$

and

$$\hat{T}(E2) = e^{(2)}_n \left(e^{(2)}_{\pi_n} \hat{Q}_\pi + e^{(2)}_{\nu_n} \hat{Q}_\nu\right) + e^{(2)}_I \left(e^{(2)}_{\pi_I} \hat{Q}_\pi + e^{(2)}_{\nu_I} \hat{Q}_\nu\right), \quad (12)$$

where the operator $\hat{Q}$ is defined in Eq.(7). For the calculations, the same values for the χ parameters are used in the Hamiltonian as for the electromagnetic transition rates (the consistent Q formalism). The parameters used, taken from Ref. [50], where they were determined both phenomenologically and also using an OAI mapping procedure [51,52], are listed in Table V.

The experimental $B(E2; 2^+_1 \rightarrow 0^+_{\rm gs})$ and $B(M1; 1^+_1 \rightarrow 0^+_{\rm gs})$ values were used to determine the $E2$ effective charges and the boson g factor. The $E0$ effective charges were taken from the work of Giannatiempo *et al.* [10], where fits were performed

TABLE V. Values of parameters used in the IBM-II calculations. The values listed are taken from Ref. [39]. Minor adjustments of the effective $E2$ boson charges (in e b) and the effective boson g factors (in μ_N) have been made to reproduce the $B(E2; 2_1^+ \rightarrow 0_{gs}^+)$ and $B(M1; 1_1^+ \rightarrow 0_{gs}^+)$ values. All values are in MeV, except χ, which is dimensionless. The $E0$ effective charges are in e fm^2.

Normal configuration		Intruder configuration		Mixing parameters	
Parameter	Value	Parameter	Value	Parameter	Value
ϵ_d	0.80	ϵ_d	0.50	α	0.16
κ	−0.14	κ	−0.17	β	0.08
χ_ν	0.10	χ_ν	0.10	Δ	4.0
χ_π	−0.90	χ_π	0.40	$e_I^{(2)}/e_n^{(2)}$	1.35
$C_{0\nu}$	−0.30	$C_{0\nu}$	−0.30	g_I/g_n	1
$C_{2\nu}$	−0.10	$C_{2\nu}$	−0.10	$e_I^{(0)}/e_n^{(0)}$	1
$C_{4\nu}$	0.00	$C_{4\nu}$	0.15		
ξ_1	0.24	ξ_1	0.24		
ξ_2	0.04	ξ_2	0.04		
ξ_3	0.24	ξ_3	0.24		
$e_{\nu_n}^{(2)}$	0.0748	$e_{\nu_I}^{(2)}$	0.0748		
$e_{\pi_n}^{(2)}$	0.1364	$e_{\pi_I}^{(2)}$	0.1364		
g_{ν_n}	−0.0956	g_{ν_I}	−0.0956		
g_{π_n}	1.2431	g_{π_I}	1.2431		
$e_{\nu_n}^{(0)}$	0.25	$e_{\nu_I}^{(0)}$	0.25		
$e_{\pi_n}^{(0)}$	0.10	$e_{\pi_I}^{(0)}$	0.10		

to the ^{110,112,114}Cd isotopes. The parameters listed in Table V are slightly different from the parameters used by Heyde and co-workers [8,9] but very similar to those used by Garrett *et al.* [39]. The value of the parameter χ_π describes the evolution of shape from SU(3) to O(6) [9]. Heyde *et al.* used $\chi_\pi = -0.2$ and $\chi_\pi = 0$ [9] in ^{114}Cd, whereas Garrett *et al.* found the best values are $\chi_\pi = -0.9$ and $\chi_\pi = 0.4$ in ^{112}Cd [39] for the respective normal and intruder configurations. We have adopted the parameters similar to those used by Garrett *et al.* to draw a consistent picture of the Cd nuclei. The results of the calculations for the states below 1.5 MeV (i.e., the two-phonon states and the first two members of the intruder band) are shown in Fig. 12 compared with the experimental values. The $B(E2)$ values, which could not be obtained in the present measurement because of the detection threshold, were taken from Ref. [36] and the experimental $E0$ values were taken from Ref. [12]. The transitions with $B(E2)$ strengths <0.1 W.u. are not labeled.

For the $E2$ transitions, the $B(E2; 2_2^+ \rightarrow 2_1^+)$ value is observed to be much less (22 ± 6 W.u.) than predicted (46 W.u.), whereas the $B(E2; 0_3^+ \rightarrow 2_2^+)$ value is observed to be much larger (127 ± 16 W.u.) [36] than predicted (64 W.u.). The situation is very similar to that observed by Garrett *et al.* [39] for ^{112}Cd, although the level of discrepancy between the experimental and predicted values is much higher in the case of ^{114}Cd. The calculated $B(M1; 2_3^+ \rightarrow 2_1^+)$ value is more than a factor of 2 larger than the $B(M1; 2_2^+ \rightarrow 2_1^+)$ value, whereas experimentally the reverse is true. Thus discrepancies between experiment and calculation emerge even at the two-phonon level. The absence of the $0_3^+ \rightarrow 2_1^+$ transition can only be reproduced by a destructive interference between the two-phonon and intruder transition amplitudes; even a slight change in the parameters results in a collective $0_3^+ \rightarrow 2_1^+$ transition that is not experimentally observed. A similar vanishing of the $0_3^+ \rightarrow 2_1^+$ transition in other Cd isotopes (see, e.g., Ref. [39]) remains one of the outstanding problems with the phonon-intruder picture. For the $E0$ transitions, good agreement between the experimental and predicted values has been observed for ^{112}Cd [39], whereas in ^{114}Cd, the predicted values are much higher compared to the experimental results, except for the transition from the 2_3^+ state to the 2_2^+ state. It is interesting though that the relative $E0$ intensities of the three transitions, $\rho^2(E0; 0_2^+ \rightarrow 0_1^+)$, $\rho^2(E0; 0_3^+ \rightarrow 0_1^+)$, and $\rho^2(E0; 2_3^+ \rightarrow 2_1^+)$ are almost half of the predicted values, whereas $\sim$20 times stronger strength compared to the predicted value has been observed for the $2_3^+ \rightarrow 2_2^+$ transition.

Figure 13 displays the calculated levels with *selected* $E2$ decay branches. For the experimental data (shown in Fig. 9) the levels that have, or that may be reasonably *expected* to have, collective γ decays above several Weisskopf units have been selected. For the calculated level scheme, an approximate correspondence is attempted to match the experimental level scheme. The low-energy transitions, likely to be below the observational threshold, are removed. Relatively good agreement in the excitation energies is seen between the observed and predicted levels. It is clear that there are predicted to be numerous very collective transitions occurring at high excitation energy. Experimentally, it seems to be more difficult to observe these types of transitions because of the increased competition with noncollective, high-energy branches. In the excitation energy region expected for the three-phonon states, near 1.9 MeV, a candidate for the 0^+

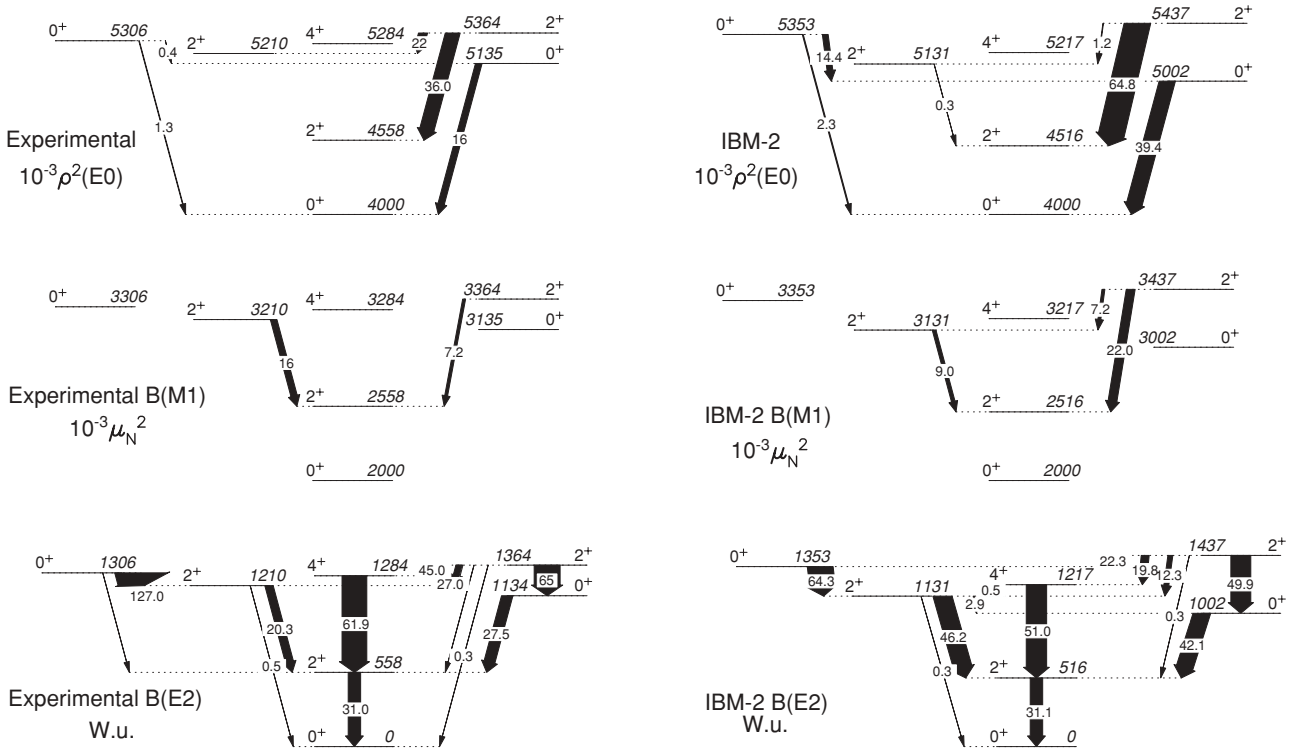

FIG. 12. Results of IBM-II calculations (described in the text) for levels in ^{114}Cd compared with experimental results (right). The top panel displays the $E0$ transitions labeled by their $10^{-3}\rho^2(E0)$ values; in the middle panel the transitions are labeled by their $B(M1)$ values in units of 10^{-3} μ_N^2, and in the bottom by their $B(E2)$ values, where greater than 0.1 W.u.

member is the level observed at 1860 keV. The 1860-keV 0^+ level has a relative $B(E2;0^+ \rightarrow 2_I^+)$ value that is nearly a factor of 10 larger than the $B(E2;0^+ \rightarrow 2_{1\text{ph}}^+)$ value and no transition from this level to the two-phonon level has been observed. This effectively rules out its identification as the 0^+ three-phonon level that is calculated to be at 1774 keV and to have a $B(E2;0^+ \rightarrow 2_{2\text{ph}}^+)$ value similar to the $B(E2;0^+ \rightarrow 2_I^+)$ one. The 4_2^+ level observed at 1732 keV has its favored decay to the 2_I^+ level, indicating its intruder character, consistent with the calculated 4_3^+ level at 2008 keV. The observed 4_3^+ level at 1932 keV has favored decay to the 2_I^+ level along with strong branches to the two-phonon states. This decay pattern is in better agreement with the decay pattern of the calculated 4_2^+ state at 1785 keV. This situation is analogous to that of the 4^+ three-phonon and intruder levels in ^{112}Cd [39]. It is believed that the strong mixing between the $4_{3\text{ph}}^+$ "normal" state and 4_I^+ intruder state, combined with the mixing between the $2_{3\text{ph}}^+$ level and 2_I^+ intruder state, strongly perturbs the decay patterns in a nonintuitive way. Constructive interference occurs in the transition matrix elements for decay from the 4_2^+

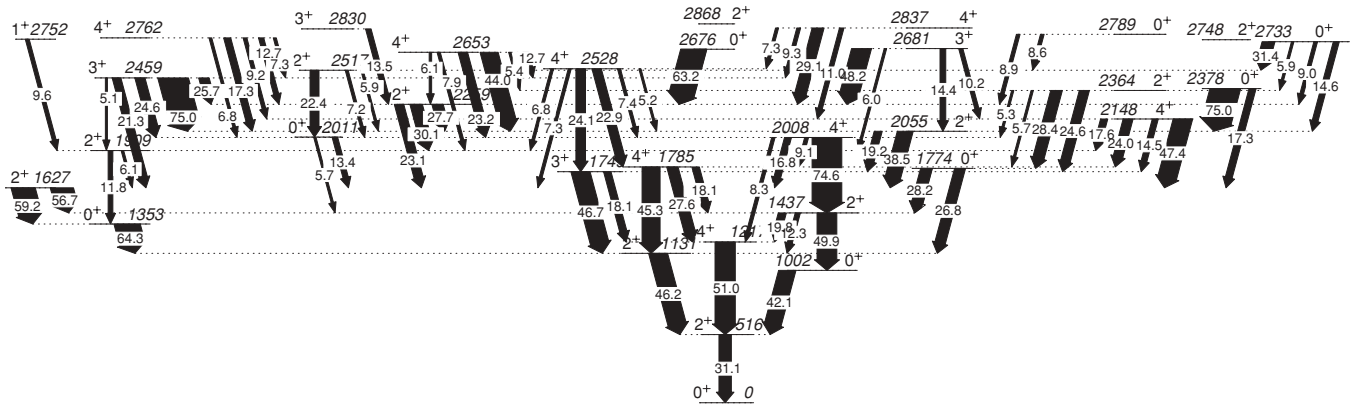

FIG. 13. Results of IBM-II calculations for $E2$ decays from selected levels (see text). Only transitions with $B(E2)$ values greater than 5.0 W.u. are shown and are labeled in Weisskopf units.

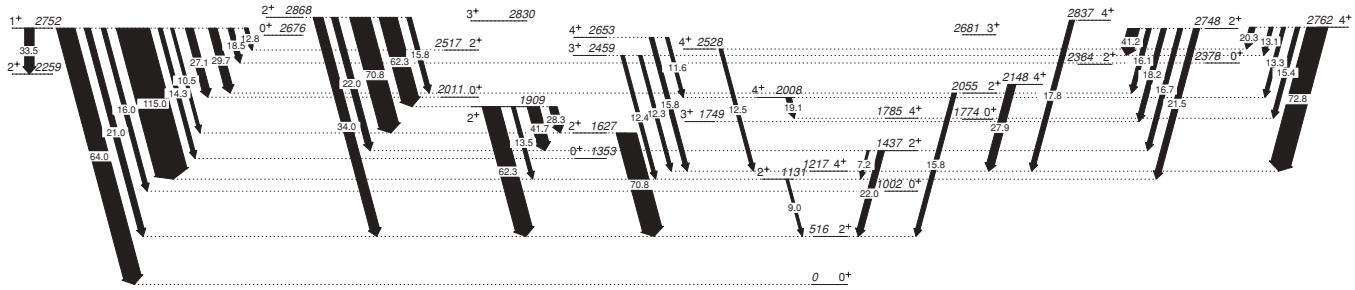

FIG. 14. Results of IBM-II calculations for selected levels and transitions. Only transitions with $B(M1)$ values greater than 0.001 μ_N^2 are shown and are labeled in units of 10^{-3} μ_N^2.

level, whereas for the 4_3^+ level destructive interference occurs. However, reversing the order of the levels in such a way is not yet fully understood. Thus, we agree that, as observed in the case of ^{112}Cd, the decay pattern of the 4^+ three-phonon and the intruder levels in ^{114}Cd [39] cannot be satisfactorily reproduced by the current model calculations.

As already discussed, none of the observed 2^+ levels near 1.9 MeV have decay patterns matching that expected for the 2^+ member of the three-phonon multiplet. The results of the calculations, as displayed in Fig. 13, are not in good agreement with the experimental results displayed in Fig. 9. The 2_4^+ level is predicted low in energy and is calculated to have an enhanced decay to the 0_3^+ state and the 2_I^+ intruder levels. This level has 50% intruder components in its wave function. The experimentally observed 2_4^+ level at 1842 keV not only has strong decays to the 0_3^+ state and the 2_I^+ intruder levels but has the strongest branch to the 0_2^+ state, inconsistent with the predicted very weak $B(E2; 2_4^+ \rightarrow 0_2^+)$ value of 2 W.u. (not shown in the figure). The 2_5^+ level at 1909 keV is predicted to have the largest three-phonon component in its wave function. The observed 2_5^+ level at 2048 keV has a $B(E2; 2_5^+ \rightarrow 0_3^+)$ value of 10 ± 3 W.u., consistent with the predicted $B(E2; 2_5^+ \rightarrow 0_3^+)$ value of 11.8 W.u. The 3_1^+ level at 1864 keV has its strongest decay branch to the 2_2^+ level, which is also consistent with the calculation. However, the branch from the 3_1^+ level to the 4_1^+ level is predicted to be enhanced compared to the observation.

Figure 14 shows the results of calculated $B(M1)$ values for levels up to 3 MeV and for transition strengths above 0.001 μ_N^2. The parameters used are similar to those of Délèze *et al.* [50], but the values for the g factors have been slightly adjusted to reproduce the experimental $B(M1; 1^+ \rightarrow 0_{gs}^+)$ value of 0.064 μ_N^2. The lowest mixed-symmetry state is identified at 2219 keV and is predicted to be at 1909 keV. The calculated $2_{ms}^+ \otimes 2_{1ph}^+$ quintuplet, the main source of $M1$ strength, is expected to be located in a series of states in the vicinity of 2.8 MeV as displayed in Fig. 14. The 1^+ member, calculated to be at 2752 keV, is experimentally observed at 2800 keV. The experimental data as shown in Fig. 11 reveal a number of enhanced $M1$ transitions between low-lying levels that cannot be accounted for in the IBM-II calculations. The enhanced $M1$ strengths at low excitation energy can be understood as a result of two-quasiparticle excitations, which can also possess significant $M1$ strengths, and are clearly outside the IBM-II model space. Experimentally, mixed-symmetry states can only be identified by their enhanced $M1$ decays, which in the Cd nuclei are observed to be rather weak. Hence, in the presence of quasiparticle contributions, it is believed to be rather difficult to identify the $2_{1ph}^+ \otimes 2_{ms}^+$ quintuplet. These quasiparticle contributions, however, should not overly influence the transition strength of the $1_{ms}^+ \rightarrow 0_{gs}^+$ transition or the assignment of the 2_{ms}^+ state [39].

IV. SUMMARY AND CONCLUSIONS

We have studied the low-spin states of ^{114}Cd below 3.5 MeV with the $(n, n'\gamma)$ reaction. Although the phonon picture is consistent with the higher spin states, explaining the phonon origin of the lower spin states, especially 0^+ and 2^+ states, is a challenge. For the three-phonon quintuplet, except the 2^+ member, this present measurement agrees with the previous assignments. The 2_4^+ level, which was assigned as the 2^+ member of the three-phonon quintuplet, has been assigned as the intruder state whereas the 2_5^+ level has been proposed as a member of the three-phonon quintuplet in the present measurement. We have supported the origin of the 4^+ state at 2391 keV as a hexadecapole excitation. The 1^+ state at 2800 keV has been proposed as the dipole member of the two-phonon mixed-symmetry $(2_{ms}^+ \otimes 2_{1ph}^+)$ quintuplet. Although relatively good agreement has been obtained between the experimental results and the predictions of the IBM calculation in the framework of the U(5)-O(6) symmetry limit for the excitation energies, the observed $E2$ and $M1$ decay patterns could not be reproduced in the calculation, indicating that some physics might be missing in the calculation. Clearly, a hexadecapole excitation or g boson needs to be included in the calculation. Inclusion of two-quasiparticle excitation may also improve the agreement between the observed and calculated $M1$ strengths.

ACKNOWLEDGMENTS

We sincerely thank H. E. Baber whose maintenance and development allowed smooth operation of the Van de Graaff accelerator. This work was partly supported by the U. S. National Science Foundation under Grant No. PHY-0652415.

[1] R. F. Casten, J. Jolie, H. G. Börner, D. S. Brenner, N. V. Zamfir, W.-T. Chou, and A. Aprahamian, Phys. Lett. **B297**, 19 (1992).
[2] J. Kern, P. E. Garrett, J. Jolie, and H. Lehmann, Nucl. Phys. **A593**, 21 (1995).
[3] K. Heyde, P. Van Isacker, M. Waroquier, G. Wenes, and M. Sambataro, Phys. Rev. C **25**, 3160 (1982).
[4] R. W. Bauer, J. A. Becker, I. D. Proctor, D. J. Decman, R. G. Lanier, and J. A. Cizewski, Phys. Rev. C **34**, 1110 (1986).
[5] H. T. Fortune, Phys. Rev. C **35**, 2318 (1987).
[6] H. Lehmann and J. Jolie, Nucl. Phys. **A588**, 623 (1995).
[7] R. F. Casten and N. V. Zamfir, Phys. Rep. **264**, 81 (1996).
[8] J. Jolie and K. Heyde, Phys. Rev. C **42**, 2034 (1990).
[9] K. Heyde, C. De Coster, J. Jolie, and J. L. Wood, Phys. Rev. C **46**, 541 (1992).
[10] A. Giannatiempo, A. Nannini, A. Perego, and P. Sona, Phys. Rev. C **44**, 1844 (1991).
[11] M. Kadi, N. Warr, P. E. Garrett, J. Jolie, and S. W. Yates, Phys. Rev. C **68**, 031306(R) (2003).
[12] A. Mheemeed, K. Schreckenbach, G. Barreau, H. R. Faust, H. G. Börner, R. Brissot, P. Hungerford, H. H. Schmidt, H. J. Scheerer, T. Von Egidy, K. Heyde, J. L. Wood, P. Van Isacker, M. Waroquier, G. Wenes, and M. L. Stelts, Nucl. Phys. **A412**, 113 (1984).
[13] C. Fahlander, A. Bäcklin, L. Hasselgren, A. Kavka, V. Mittal, L. E. Svensson, B. Varnestig, D. Cline, B. Kotlinski, H. Grein, E. Grosse, R. Kulessa, C. Michel, W. Spreng, H. J. Wollersheim, and J. Stachel, Nucl. Phys. **A485**, 327 (1988).
[14] J. R. Hurd, H. T. Fortune, J. D. Zumbro, and C. P. Browne, Phys. Rev. C **37**, 2334 (1988).
[15] P. H. Regan, C. W. Beausang, N. V. Zamfir, R. F. Casten, Jing-ye Zhang, A. D. Yamamoto, M. A. Caprio, G. Gürdal, A. A. Hecht, C. Hutter, R. Krücken, S. D. Langdown, D. A. Meyer, and J. J. Ressler, Phys. Rev. Lett. **90**, 152502 (2003).
[16] A. Gade, J. Jolie, and P. von Brentano, Phys. Rev. C **65**, 041305(R) (2002).
[17] F. Corminboeuf, T. B. Brown, L. Genilloud, C. D. Hannant, J. Jolie, J. Kern, N. Warr, and S. W. Yates, Phys. Rev. Lett. **84**, 4060 (2000).
[18] F. Corminboeuf, T. B. Brown, L. Genilloud, C. D. Hannant, J. Jolie, J. Kern, N. Warr, and S. W. Yates, Phys. Rev. C **63**, 014305 (2000).
[19] H. Lehmann, P. E. Garrett, J. Jolie, C. A. McGrath, M. Yeh, and S. W. Yates, Phys. Lett. **B387**, 259 (1996).
[20] A. Aprahamian, D. S. Brenner, R. F. Casten, R. L. Gill, and A. Piotrowski, Phys. Rev. Lett. **59**, 535 (1987).
[21] D. Bandyopadhyay, C. C. Reynolds, C. Fransen, N. Boukharouba, M. T. McEllistrem, and S. W. Yates, Phys. Rev. C **67**, 034319 (2003).
[22] D. Bandyopadhyay, C. C. Reynolds, S. R. Lesher, C. Fransen, N. Boukharouba, M. T. McEllistrem, and S. W. Yates, Phys. Rev. C **68**, 014324 (2003).
[23] P. E. Garrett, N. Warr, and S. W. Yates, J. Res. Natl. Inst. Stand. Technol. **105**, 141 (2000).
[24] S. W. Yates, T. B. Brown, C. D. Hannant, J. R. Vanhoy, and N. Warr, Heavy Ion Phys. **12**, 295 (2000).
[25] E. Sheldon and V. C. Rogers, Comput. Phys. Commun. **6**, 99 (1973).
[26] T. Belgya, G. Molnár, and S. W. Yates, Nucl. Phys. **A607**, 43 (1996).
[27] K. B. Winterbon, Atomic Energy of Canada Limited Report, AECL-4829.
[28] K. B. Winterbon, Nucl. Phys. **A246**, 293 (1975).
[29] C. Kohstall, D. Belic, P. von Brentano, C. Fransen, A. Gade, R.-D. Herzberg, J. Jolie, U. Kneissl, A. Linnemann, A. Nord, N. Pietralla, H. H. Pitz, M. Scheck, F. Stedile, V. Werner, and S. W. Yates, Phys. Rev. C **72**, 034302 (2005).
[30] J. L. Wood, E. F. Zganjar, C. De Coster, and K. Heyde, Nucl. Phys. **A651**, 323 (1999).
[31] H. W. Fielding, R. E. Anderson, C. D. Zafiratos, D. A. Lind, F. E. Cecil, H. H. Wieman, and W. P. Alford, Nucl. Phys. **A281**, 389 (1977).
[32] R. M. A. L. Petit, B. W. van der Pluymt, P. J. van Hall, S. S. Kleinll, W. H. L. Moonen, G. J. Nijgh, C. W. A. M. van Overveld, and O. J. Poppema, J. Phys. G **20**, 1955 (1994).
[33] R. A. Meyer and L. Peker, Z. Phys. A **283**, 379 (1977).
[34] K. Heyde, J. Jolie, R. Fossion, S. De Baerdemacker, and V. Hellemans, Phys. Rev. C **69**, 054304 (2004).
[35] S. Y. Araddad, A. M. Demidov, O. K. Zhuravlev, S. M. Zlitni, V. A. Kurkin, and J. M. Rateb, Yad. Fiz. **46**, 40 (1987).
[36] J. Blachot, Nucl. Data Sheets **97**, 593 (2002).
[37] D. F. Kusnezov, computer code OCTLAN, 1987 (unpublished); computer code OCTUPOLE, 1987 (unpublished); computer code OCTEM, 1987 (unpublished).
[38] E. Lund and B. Fogelberg, Z. Phys. A **315**, 295 (1984).
[39] P. E. Garrett, K. L. Green, H. Lehmann, J. Jolie, C. A. McGrath, M. Yeh, and S. W. Yates, Phys. Rev. C **75**, 054310 (2007).
[40] P. Hungerford and W. D. Hamilton, J. Phys. G **8**, 1107 (1982).
[41] M. Koike, I. Nonaka, J. Kokame, H. Kamitsubo, Y. Awaya, T. Wada, and H. Nakamura, Nucl. Phys. **A125**, 161 (1969).
[42] D. C. J. M. Hageman, M. N. Harakeh, R. H. Siemssen, and S. Y. van Der Werf, Nucl. Phys. **A290**, 1 (1977).
[43] R. De Leo, N. Blasi, S. Micheletti, M. Pignanelli, W. T. A. Borghols, J. M. Schippers, S. Y. Van der Werf, G. Maino, and M. N. Harakeh, Nucl. Phys. **A504**, 109 (1989).
[44] A. Gade, A. Fitzler, C. Fransen, J. Jolie, S. Kasemann, H. Klein, A. Linnemann, V. Werner, and P. von Brentano, Phys. Rev. C **66**, 034311 (2002).
[45] A. Gade, D. Belic, P. von Brentano, C. Fransen, H. von Garrel, J. Jolie, U. Kneissl, C. Kohstall, A. Linnemann, H. H. Pitz, M. Scheck, F. Stedile, and V. Werner, Phys. Rev. C **67**, 034304 (2003).
[46] P. von Brentano, J. Eberth, J. Enders, L. Esser, R.-D. Herzberg, N. Huxel, H. Meise, P. von Neumann-Cosel, N. Nicolay, N. Pietralla, H. Prade, J. Reif, A. Richter, C. Schlegel, R. Schwengner, S. Skoda, H. G. Thomas, I. Wiedenhöver, G. Winter, and A. Zilges, Phys. Rev. Lett. **76**, 2029 (1996).
[47] H. Maser, N. Pietralla, P. von Brentano, R.-D. Herzberg, U. Kneissl, J. Margraf, H. H. Pitz, and A. Zilges, Phys. Rev. C **54**, R2129 (1996).
[48] A. Gade, H. Klein, N. Pietralla, and P. von Brentano, Phys. Rev. C **65**, 054311 (2002).
[49] T. Otsuka, computer programs NPBOS and NPEM, 1977.
[50] M. Délèze, S. Drissi, J. Kern, P. A. Tercier, J.-P. Vorlet, J. Rikovska, T. Otsuka, S. Judge, and A. Williams, Nucl. Phys. **A551**, 269 (1993).
[51] T. Otsuka, A. Arima, F. Iachello, and I. Talmi, Phys. Lett. **B76**, 139 (1978).
[52] T. Otsuka, A. Arima, and F. Iachello, Nucl. Phys. **A309**, 1 (1979).